Journal of Neuroinflammation

RESEARCH

Open Access

Inhibition of ANGPTL8 protects against diabetes-associated cognitive dysfunction by reducing synaptic loss via the PirB signaling pathway

Xiaoyu Meng[1,2†], Danpei Li[1,2†], Ranran Kan[1,2], Yuxi Xiang[1,2], Limeng Pan[1,2], Yaming Guo[1,2], Peng Yu[1,2], Peiqiong Luo[1,2], Huajie Zou[1,2], Li Huang[1,2], Yurong Zhu[1,2], Beibei Mao[1,2], Yi He[1,2], Lei Xie[1,2], Jialu Xu[1,2], Xiaoyan Liu[3], Wenjun Li[4], Yong Chen[1,2], Suiqiang Zhu[3], Yan Yang[1,2*] and Xuefeng Yu[1,2*]

Abstract

Background Type 2 diabetes mellitus (T2D) is associated with an increased risk of cognitive dysfunction. Angiopoietin-like protein 8 (ANGPTL8) is an important regulator in T2D, but the role of ANGPTL8 in diabetes-associated cognitive dysfunction remains unknown. Here, we explored the role of ANGPTL8 in diabetes-associated cognitive dysfunction through its interaction with paired immunoglobulin-like receptor B (PirB) in the central nervous system.

Methods The levels of ANGPTL8 in type 2 diabetic patients with cognitive dysfunction and control individuals were measured. Mouse models of diabetes-associated cognitive dysfunction were constructed to investigate the role of ANGPTL8 in cognitive function. The cognitive function of the mice was assessed by the Barnes Maze test and the novel object recognition test, and levels of ANGPTL8, synaptic and axonal markers, and pro-inflammatory cytokines were measured. Primary neurons and microglia were treated with recombinant ANGPTL8 protein (rA8), and subsequent changes were examined. In addition, the changes induced by ANGPTL8 were validated after blocking PirB and its downstream pathways. Finally, mice with central nervous system-specific knockout of *Angptl8* and $PirB^{-/-}$ mice were generated, and relevant in vivo experiments were performed.

Results Here, we demonstrated that in the diabetic brain, ANGPTL8 was secreted by neurons into the hippocampus, resulting in neuroinflammation and impairment of synaptic plasticity. Moreover, neuron-specific *Angptl8* knockout prevented diabetes-associated cognitive dysfunction and neuroinflammation. Mechanistically, ANGPTL8 acted in parallel to neurons and microglia via its receptor PirB, manifesting as downregulation of synaptic and axonal markers in neurons and upregulation of proinflammatory cytokine expression in microglia. In vivo, $PirB^{-/-}$ mice exhibited resistance to ANGPTL8-induced neuroinflammation and synaptic damage.

†Xiaoyu Meng and Danpei Li have contributed equally to this study.

*Correspondence:
Yan Yang
yangyan6910@163.com
Xuefeng Yu
xfyu188@163.com
Full list of author information is available at the end of the article

Conclusion Taken together, our findings reveal the role of ANGPTL8 in the pathogenesis of diabetes-associated cognitive dysfunction and identify the ANGPTL8-PirB signaling pathway as a potential target for the management of this condition.

Keywords Diabetes-associated cognitive dysfunction, Angiopoietin-like protein 8, Paired immunoglobulin-like receptor B, Neurons, Microglia

Introduction

Substantial epidemiological evidence supports the association of diabetes mellitus with decrements in cognitive function and changes in brain structure [1]. Increasingly, cognitive dysfunction is recognized as an important comorbidity of type 2 diabetes mellitus (T2D), referred to as 'diabetes-associated cognitive dysfunction' [2]. Changes in hippocampal neurons have been reported in patients and animals with diabetes, including damage to synaptic structures, axonal degeneration and loss of neurons [3–6]. Moreover, the expression of proinflammatory cytokines in the brain is increased and plays a vital role in cognitive impairment through toxic effects on neurons, participation in dendrite clearance, or limiting synaptic connections [7, 8]. In light of the effect of cognitive dysfunction on affected individuals and society, a preventive treatment for cognitive dysfunction in diabetes is needed, particularly for retardation of progress to the more severe stages. However, our understanding of the potential mechanisms and therapeutic targets underlying cognitive dysfunction in diabetes is incomplete.

Angiopoietin-like protein 8 (ANGPTL8), also described as betatrophin, lipasin, and refeeding induced in fat and liver (RIFL), is a new nutritionally regulated liver-enriched factor with a role in lipid metabolism [9]. ANGPTL8 was also shown to be associated with diabetes and insulin resistance [10]. Circulating ANGPTL8 levels were significantly increased in patients with T2D [11, 12]. Previous studies have shown that ANGPTL8 is found in the brain [13, 14]. However, the source of ANGPTL8 in the brain remains to be elucidated in the context of diabetes-associated cognitive dysfunction.

Our previous study suggested that ANGPTL8 interacts with its receptor paired immunoglobulin-like receptor B (PirB) and regulates downstream signaling pathways [15]. Notably, PirB and its human ortholog receptor (leukocyte immunoglobulin-like receptor B, LILRB) are distributed in various hematopoietic cells and extensively in different regions of the injured central nervous system (CNS) [16]. Emerging evidence suggests that PirB contributes to the neuropathology of human Alzheimer's disease [16, 17] (including synaptic loss and neurotransmitter release), hippocampal function decline, and aging-induced cognitive dysfunction [18]. Although an association between PirB and cognitive dysfunction has been reported, the mechanisms by which PirB signals and which ligands are involved have yet to be determined.

Considering this, we speculate that ANGPTL8 is involved in the mechanisms of diabetes-associated cognitive dysfunction through interaction with PirB in the CNS. In this study, we demonstrated the role of ANGPTL8 in regulating synaptic plasticity and microglial inflammatory activity and identified the ANGPTL8-PirB signaling pathway as a potential target for the management or treatment of diabetes-associated cognitive dysfunction.

Materials and methods

Participants

The present study consisted of 30 individuals from the Tongji Hospital of Wuhan, including 20 patients with T2D and 10 individuals without T2D as controls. The inclusion and exclusion criteria are listed in the *Supplementary Methods*. The global cognitive function of all subjects was measured by the Mini-Mental State Examination (MMSE) [19] and Montreal Cognitive Assessment (MoCA, available at www.mocatest.org) [20]. Higher MMSE and MoCA scores indicated better cognition; the MMSE cutoff score for dementia was 23/24 [21], and the MoCA cutoff score for mild cognitive impairment (MCI) was 25/26 [22]. Cognitive dysfunction was assessed on a case-by-case basis by the study neuropsychologist following stratification of scores according to education. The serum and cerebrospinal fluid (CSF) of subjects were collected. The study protocols (approval number: TJ-IRB20230452) were approved by the Committee on Human Research at Tongji Hospital, Tongji Medical College, Huazhong University of Science and Technology. All participants provided written informed consent.

Animals

All animal protocols were approved by the Institutional Animal Care and Use Committee of the Institute of Model Animals of Tongji Hospital, Huazhong University of Science and Technology. The animals received humane care according to the criteria outlined in the Guide for the Care and Use of Laboratory Animals prepared by the National Academy of Sciences and published by the National Institutes of Health [23].

The mice were given free access to food and water and housed in a temperature-controlled environment (23 ± 2 °C) with a 12-h/12-h light/dark cycle. Several animal models were used in this study, including wild-type (WT) mice, db/m, db/db, CNS-specific *Angptl8* depletion mice and PirB knockout mice. Six-month-old male db/m and db/db mice (BKS-*Lepr*^{em2Cd479}/*Gpt*, strain number: T002407) were purchased from GemPharmatech Co., Ltd. (Jiangsu, China). Male CNS-specific *Angptl8*-depletion (*Angptl8*$^{Nestin\ CKO}$) mice on a C57BL/6 genetic background were generated by Cyagen Biosciences Inc. (Guangzhou, China) using CRISPR/Cas9-mediated genome engineering. The mouse *Angptl8* gene (GenBank accession number: NM_001080940.1) is located on mouse chromosome 9, and 4 exons have been identified, with the ATG start codon in exon 1 and the TGA stop codon in exon 4 (transcript: ENSMUST00000058777). Exons 1–2 were selected as the conditional knockout (cKO) region. Deletion of this region should result in the loss of function of the mouse *Angptl8* gene. For the genetically targeted model, Cas9 and guide RNA (gRNA) were coinjected into fertilized mouse eggs to generate targeted knockout offspring. *Angptl8*$^{Nestin\ CKO}$ mice were generated by intercrossing these heterozygous transgenic founder mice with homozygous Nestin-Cre mice. Genomic DNA extracted from tail biopsies was used for genotyping with a PCR primer set (P1: 5′-ATG GCAGCCTATGGAAATAAAAGG-3′, P2: 5′-TCT TCATATTGAGCTGGCTCTGGA-3′) that amplified a 168-bp band in samples from mice with the wild-type allele and a 202-bp band in samples from mice with the *Angptl8* floxed allele. Moreover, genomic DNA extracted from tail biopsies was used for genotyping with a PCR primer set (P1: 5′-CCTTCCTGAAGC AGTAGAGCA-3′, P2: 5′-GCCTTATTGTGGAAGGAC TG-3′; P3: 5′-TTGCTAAAGCGCTACATAGGA-3′, P2: 5′-GCCTTATTGTGGAAGGACTG-3′) that amplified a 246-bp band in samples from mice with the wild-type allele and a 150-bp band in samples from mice with the Nestin-Cre allele. PirB knockout mice (*PirB*$^{-/-}$) were purchased from Cyagen Biosciences Inc. Models of diabetes-associated cognitive dysfunction were induced by feeding 8-week-old male C57BL/6J mice a high-fat diet (HFD, D12492, Research Diets, 60 kcal% fat, 20 kcal% carbohydrate, and 20 kcal% protein, Jiangsu Xietong, Inc., Nanjing, China) for 9 months. Control mice were maintained on a normal diet (ND, 10 kcal% fat, 70 kcal% carbohydrate, and 20 kcal% protein, Jiangsu Xietong, Inc., Nanjing, China, Cat# SWS9102).

According to previous studies, neuroinflammation and memory impairment occurred in mice fed a HFD for 4–6 months [24, 25] and db/db mice fed a ND for over 6 months [26–28]. Therefore, cognitive dysfunction and neuropathology could occur in the diabetic mice in this study.

Stereotaxic injections of recombinant ANGPTL8 (rA8)

For injection of rA8 into the CA1 region of the hippocampus, 8-week-old mice were anesthetized using a mixture of ketamine (90 mg/kg) and xylazine (2.7 mg/kg) and placed in a stereotaxic device (Kopf Instruments). Then, 0.5 μl rA8 (2 μg/μl) or scrambled protein was injected into the CA1 region of the bilateral hippocampus with a 10 μl microsyringe (Hamilton, Fisher Labosi, France) (0.1 μl/min, single dose). Hippocampal CA1 injections were made at the following coordinates relative to the bregma: − 2 mm at the anterior/posterior axis, ± 1.8 mm at the lateral/medial axis and -1.5 mm at the dorsal/ventral axis. Before returning to the original coordinates and administering the injection, the syringe was inserted to an extra depth of 0.5 mm [29, 30]. The syringe was left in place for an additional 5 min (min) to allow rA8 to spread into the brain. One month after injection, behavioral tests were performed in mice before tissue collection [30].

Stereotaxic injections of AAV9-Nestin-Cre

For injection of AAV-Nestin-Cre into the hippocampal CA1 region, the mice were anesthetized using a mixture of ketamine (90 mg/kg) and xylazine (2.7 mg/kg) and placed in a stereotaxic device (Kopf Instruments). Then, 0.5 μl AAV9-Nestin-Cre virus (7.77×10^{12} v.g./ml, Obio Technology, Shanghai, China) or control virus was injected into the bilateral hippocampal CA1 region with a 10 μl microsyringe (Hamilton, Fisher Labosi, France) (0.1 μl/min, single dose).

Glucose tolerance test (GTT) and insulin tolerance test (ITT)

To perform in vivo glucose tolerance tests (GTTs) and insulin tolerance tests (ITTs), mice were intraperitoneally injected with 1.5 g of glucose (Sigma–Aldrich Co. St. Louis, MO, USA) or 1 U insulin (Novolin R, Novo Nordisk Co., Bagsvaerd, Denmark) per kg body weight, respectively. Corresponding blood glucose concentrations were examined at the indicated time points [15, 31].

Behavioral assessment

The behavioral tests used in this study were the open field test, novel object recognition test and Barnes maze test. The open field test was conducted on the first day, and the novel object recognition test was performed with 2 trials on the second day. The Barnes maze test was conducted over the following 5 days. These behavioral tests were adapted according to previous studies [27, 28, 32].

Open field test

The open field test was used to assess general activity in rodents [27]. Each mouse was placed in the center of a square open field box (45 × 45 × 45 cm), which was placed in a quiet and well-lit room, and allowed to roam freely for 10 min with an overhead video camera recording the movements. The total distance moved as well as the velocity of each mouse during that period was recorded and analyzed by a computerized EthoVision detection system (Noldus, Wageningen, The Netherlands). The area between each test was cleaned with 70% ethanol.

Novel object recognition test

Based on the spontaneous tendency of rodents to spend more time exploring a novel object than a familiar object, the novel object recognition test was used to evaluate hippocampal- and cortex-dependent contextual learning and recognition memory in rodents. The test was conducted in the same area as the open field test described above. In the first trial, mice were individually allowed to investigate two identical objects for 5 min and then returned to their home cage for an interval of 30 min. During the second trial, mice were allowed to explore the objects with one familiar and one novel object for 5 min. All trials were recorded and analyzed by automated EthoVision tracking software (Noldus). The recognition index was then calculated as the difference in time spent exploring the novel and familiar objects or the frequency of explorations of each object using the formulas: [(frequency exploring novel object−frequency exploring familiar object)/(total frequency exploring both objects)*100] or [(time exploring novel object−time exploring familiar object)/(total time exploring both objects)*100], respectively [33]. The recognition index was used as a measure of memory.

Barnes maze test

The Barnes maze was used to test spatial learning and memory [28, 32]. Spatial learning and memory ability were evaluated using a Barnes maze, which was a dark gray circular platform (100 cm in diameter, raised 90 cm above the floor) that contained 20 holes (5 cm in diameter). One of the holes led to an escape box. There were spatial cues, which were visible to the mice, located in fixed positions around the platform in the testing room. Bright light served as a mildly aversive environmental stimulus from which mice tried to escape. The simplified Barnes maze test included spatial acquisition and probe trials. The mice were each given 5 min to adapt to the maze and the existence of the escape box on the first day. The first acquisition session was performed for 5 min after an intertrial interval of 30 min. The mice were gently guided to the escape box if they did not find it and stayed there for 2 min. Then, from the second to third day, two training trials (5 min per trial) with an intertrial interval of 30 min were performed in the acquisition test. On the fourth day, the mice were allowed to rest for 24 h. On the fifth day, the probe test with the escape box removed was conducted for 5 min. The errors each mouse made before locating the escape hole were recorded by a video camera and analyzed using EthoVision as an assessment of spatial memory retention.

Lipopolysaccharide (LPS) and flag-targeted recombinant ANGPTL8 protein (rA8-flag) injection

For the LPS injection experiment, 8-week-old mice were randomly divided into two groups and intraperitoneally (i.p.) injected with a dose of LPS (1 mg/kg) (Sigma) or saline (control) for 36 h before tissue collection.

rA8-flag, an exogenously labeled protein tagged with a short hydrophilic amino acid sequence, DYKDDDDK, can be detected by flow cytometry analysis, Western blotting, and immunofluorescence staining and has a negligible influence on the biological function of the recombinant protein [34]. In the rA8-flag injection experiment, two-month-old mice were randomly divided into two groups and injected i.p. with a dose of rA8-flag (1 mg/kg) or saline (control) for 8 h.

Plasma, CSF and tissue collection

After the completion of all tests, mice were anesthetized with isoflurane, and plasma and CSF were collected followed by cervical dislocation. Then, the brains were extracted and quickly dissected on ice. The right hemispheres of the brains were fixed in 4% paraformaldehyde for immunofluorescence analysis, and the hippocampus was separated from the left hemisphere and frozen at − 80 ℃ for Western blotting and quantitative polymerase chain reaction (qPCR) analysis.

Enzyme-linked immunosorbent assay (ELISA)

The serum ANGPTL8 levels of participants were quantified using commercially available ELISA kits (Eiaab Science, Wuhan, China; Catalog No. E11644h). Commercially available mouse ELISA kits (Eiaab Science Inc., Wuhan, China, Cat# E11644 m) were used to measure ANGPTL8 levels in the CSF of mice.

Hippocampal triglyceride (TG) level measurement

Hippocampal TG levels were measured using a TG assay kit (Nanjing Jiancheng Bioengineering Institute, Nanjing, China, Cat#A110-1-1). All assays and data analyses were performed according to the manufacturer's protocol.

Brain immunofluorescence

The paraffin-embedded sections were deparaffinized and stained with the following primary antibodies (pAbs) overnight at 4 ℃: an anti-ANGPTL8 rabbit pAb (Thermo Fisher Scientific, USA, Cat# PA5-38043, 1:100 dilution), an anti-PirB rat monoclonal antibody (mAb) (Thermo Fisher Scientific, USA, Cat# MA5-24049, 1:50 dilution), a PE-conjugated anti-Flag mAb (BioLegend, USA, Cat# 637310, 1:200 dilution), an anti-NeuN antibody (Servicebio, Wuhan, China, Cat#GB11138-100, 1:200 dilution), an anti-CD16/32 antibody (Abcam, Cambridge, UK, Cat# ab223200, 1:200 dilution), an anti-CD206 antibody (AbD Serotec, Oxford, UK, Cat# MCA2235T, 1:200 dilution), an anti-IBA-1 antibody (Servicebio, Wuhan, China, Cat# GB11105, 1:200 dilution) and an anti-CD11b antibody (Servicebio, Wuhan, China, Cat# GB11058, 1:200 dilution). After washing in phosphate-buffered saline (PBS), sections were visualized by Alexa Fluor-conjugated secondary antibody (Servicebio, Wuhan, China, Cat# GB25303, 1:200 dilution) or Cy3-conjugated secondary antibody (Servicebio, Wuhan, China, Cat# GB21303, 1:200 dilution). Nuclear counterstaining was performed using 4′,6-diamidino-2-phenylindole (DAPI), and the sections were viewed with a fluorescence microscope. Similar and comparable histological areas were selected.

Transmission electron microscopy of synapses

The hippocampus was carefully separated, rapidly cut into small pieces (1 mm^3) and then fixed in 2.5% glutaraldehyde in PBS and postfixed in 1% OsO4 at 4 ℃. After fixation, the samples were dehydrated in a graded series of alcohol and embedded in Poly/Bed 812 resin, followed by ultrathin (80-nm) sectioning with an ultramicrotome. Images were generated with a Hitachi H-7650 transmission electron microscope (Hitachi, Japan) at 80 kV. Three visual fields of each tissue section were imaged (12,000×) to produce a low-resolution map for quantitative analysis, and then high-resolution images (40,000×) were captured. Synapses were identified by the presence of synaptic vesicles and postsynaptic densities. The number of synapses was measured using ImageJ software. All electron microscopy quantification was performed by at least two independent observers who were blinded to genotype.

Nissl staining

After the mice were perfused with 0.1 mol/l PBS followed by 4% paraformaldehyde (PFA), the hippocampal tissues were immersed in 4% PFA for 24 h and transferred to 30% sucrose solution until they sank. Subsequently, the hippocampal tissues were cut into 20-um-thick sections using a freezing microtome (Thermo, USA). After the sections were incubated with 0.1% cresyl violet for 5 min at room temperature, they were rinsed in double distilled water followed by 95% ethanol, dehydrated in 100% ethanol and cleared in xylene, and covered with neutral resin. Images were acquired with a microscope (Nikon, Tokyo, Japan) and the hippocampal neurons were counted with Image J software (Media Cybernetics, Bethesda, MD, USA). Quantitative analysis of histological staining and fluorescence signals was performed by ImageJ [35].

Primary neuron and microglia culture

Hippocampi were dissected from C57BL/6J mouse pups less than 24 h old, dissociated using trypsin (2 mg/ml) and Dnase I (0.6 mg/ml), and plated at a density of 1×10^6 cells per well in 6-well plates coated with poly-L-lysine (PLL, 0.01 mg/ml, Sigma). Neurons were maintained in neurobasal medium (Gibco) supplemented with 2% B27 (Invitrogen), 1% penicillin–streptomycin (Sigma) and 0.5 mM L-glutamine at 37 ℃ in a humidified atmosphere containing 5% CO_2.

Primary microglial cultures were prepared from the cerebral cortices of postnatal day 1–2 C57BL/6J mice. Briefly, the meninges were removed from the brains, and the cortex was enzymatically dissociated (0.25% trypsin–EDTA, Sigma, St Louis, MO, USA). Then, the cells were suspended in Dulbecco's modified Eagle's medium/nutrient mixture F-12 (DMEM/F12, Gibco, Carlsbad, CA, USA) supplemented with 10% fetal bovine serum (FBS, Gibco) and seeded into PLL precoated T75 tissue culture flasks. After 3, 7, and 10 days, the culture medium was renewed. After achieving confluency at approximately 14 days in vitro, microglia were isolated from mixed glia cultures with mild trypsinization. Incubation of mixed glial cultures with a trypsin solution (0.25% trypsin–EDTA diluted 1:4 in DMEM/F12) for 15–25 min resulted in the detachment of an intact layer of cells in one piece. Microglia remained attached to the bottom of the flask. Then, microglia were collected and plated at a density of 1×10^6 cells per well in 6-well plates coated with PLL.

Recombinant ANGPTL8 protein treatment

Before rA8 treatment, the culture medium of neurons and microglia was renewed. The neurons were stimulated with 30 ng/ml, 100 ng/ml, 300 ng/ml, and 1000 ng/ml rA8 (Cusabio, Wuhan, China, Cat# CSB-MP844436MO) or scrambled ANGPTL8 after being cultured for 4–6 h for an additional 5-day period. The microglia were stimulated with 30 ng/ml, 100 ng/ml, 300 ng/ml, and 1000 ng/ml rA8 or scrambled ANGPTL8 after plating in culture plates for 1 day for an additional 24-h period.

LPS or TNF-α treatment

Before LPS treatment, the culture medium of the neurons and microglia was renewed. The neurons were stimulated

with 1000 ng/ml LPS (Sigma) or PBS after culturing for 5 days for an additional 24-h period. The microglia were stimulated with 1000 ng/ml LPS or PBS for an additional 24-h period after being plated in culture plates for 1 day.

Before TNF-α treatment, the culture medium of neurons was renewed. The neurons were stimulated with 10 ng/ml, 100 ng/ml, and 300 ng/ml TNF-α (Sigma) or scrambled TNF-α for an additional 24-h period after being cultured for 5 days.

Antibody blockade assay

Neurons and microglia were pretreated with control IgG (10 μg/ml) and anti-PirB ectodomain antibody (10 μg/ml, Thermo Fisher Scientific, MA, USA, Cat# MA5-24049) for 30 min before incubation with rA8 (1000 ng/ml).

Signaling pathway inhibitors

Neurons were pretreated with inhibitors of ERK1/2 (U0126; 10 nM, MedChem Express, NJ, USA, Cat# HY-12031) and AKT (MK-2206; 10 nM, MedChem Express, NJ, USA, Cat# HY-10358) for 30 min before incubation with rA8 (1000 ng/ml).

Microglia were pretreated with inhibitors of ERK1/2 (U0126; 10 nM, MedChem Express, NJ, USA, Cat# HY-12031), AKT (MK-2206; 10 nM, MedChem Express, NJ, USA, Cat# HY-10358), P38 (SB203580; 10 nM, MedChem Express, NJ, USA, Cat# HY-10256), or P65 (Bay11-7082; 10 nM, MedChem Express, NJ, USA, Cat# HY-13453) for 30 min before incubation with rA8 (1000 ng/ml).

RNA-sequencing analysis

Neuronal mRNA was sequenced by Shanghai Biotechnology Corporation. Differential gene expression analysis was performed using the limma R package (version 3.44.3). The fold change (FC) in expression of each gene was log2 transformed and further analyzed using RStudio version 1.1.442 (RStudio, inc., USA).

Flow cytometry

Microglia were plated in 6-well plates at 1×10^6 cells per well and collected using 0.25% trypsin–EDTA at 37 ℃ after treatment with rA8 or scrambled ANGPTL8 for 24 h. Cell suspensions were washed with flow cytometry buffer (PBS with 2% FCS, 2 mM EDTA and 25 mM HEPES, pH 7.4) and then incubated with blocking buffer (5% BSA in flow cytometry buffer) for 15 min at 4 ℃. Cells were then stained with the desired antibodies for 30 min on ice. The following controls were used: unstained cells, single-stained cells, and dead cells. The cells were gated using forward and side scatter, as well as live-dead staining using DAPI (Thermo Fisher Scientific). Cells were analyzed with FlowJo software (FlowJo). The antibodies included FITC-CD11b (BioLegend, CA, USA, #101206; 1 μg per 10^6 cells), APC-CD206 (BioLegend, CA, USA, #141707; 2 μg per 10^6 cells), and PE-Iba-1 (Cell Signaling Technology, USA, #10513; 1 μg per 10^6 cells). All antibodies were diluted according to the manufacturer's instructions. Dead cells and doublets were removed by dead-cell dye staining (Zombie Aqua Fixable Viability Kit, BioLegend, CA, USA, #B297827).

Cellular immunofluorescence

Cells were seeded in a 24-well plate with coverslips. Neurons and microglia were treated with exogenous rA8-flag (1000 ng/ml) or scrambled ANGPTL8 for 5 days and 24 h, respectively. After treatment, the cells on the coverslips were fixed with 4% paraformaldehyde at room temperature for 10 min and then permeabilized with 0.1% Triton X-100 for 15 min. A blocking step was performed with 5% bovine serum albumin (BSA) for 1 h. Subsequently, the cells were incubated with the primary antibodies overnight at 4 °C. After washing, the cells were incubated with appropriate fluorescent secondary antibodies for 1 h. After three washes, the cells on the coverslips were incubated with DAPI (5 μg/ml) at room temperature for 5 min and observed under a fluorescence microscope. The antibodies used in this study included PE-conjugated anti-Flag mAb (BioLegend, USA, Cat# 637310, 1:100 dilution), anti-PirB rat mAb (Thermo Fisher Scientific, USA, Cat# MA5-24049, 1:100 dilution), anti-βIII-tubulin rabbit mAb (Cell Signaling Technology, USA, Cat#5568, 1:200 dilution), Alexa Fluor-conjugated secondary antibody (Servicebio, Wuhan, China, Cat# GB25303, 1:500 dilution), and Cy3-conjugated secondary antibody (Servicebio, Wuhan, China, Cat# GB21303, 1:500 dilution).

RNA isolation and real-time quantitative PCR (RT–qPCR)

Total RNA was extracted using TRIzol (Thermo Fisher Scientific, MA, USA, Cat# 15596018) following the manufacturer's instructions and quantified using a Nanodrop spectrophotometer. To prepare RNA for PCR analysis, 1 μg of total RNA was converted to cDNA using Hifair® II 1st Strand cDNA Synthesis SuperMix (Yeasen, Shanghai, China, Cat#11120ES60). RT–qPCR was performed using the qPCR Hieff UNICON® qPCR SYBR Green Master Mix (Low Rox) (Yeasen, Shanghai, China, Cat#11199ES08) under the following conditions: initial denaturation at 95 °C for 30 s, 40 cycles at 95 °C for 10 s, and 60 °C for 30 s. Each sample was analyzed in triplicate. Relative mRNA levels were calculated using the $2^{-\Delta\Delta Ct}$ method and normalized to GAPDH mRNA levels. The gene-specific primer sequences are listed in *Supplementary Table 1*.

Western blotting

Cells and frozen hippocampal samples were lysed in RIPA extract buffer (Beyotime, Shanghai, China, Cat# P0013B) supplemented with protease inhibitor cocktail (MedChem Express, USA, HY-K0010), phosphatase inhibitor cocktail I (MedChem Express, USA, HY-K0021) and phosphatase inhibitor cocktail II (MedChem Express, USA, HY-K0022) according to the manufacturer's protocol. Then, the lysis buffer containing protein was centrifuged at 14,000×*g* for 15 min at 4 °C. Equal amounts of protein (20 μg) were loaded into each lane, separated by 10% SDS polyacrylamide gel electrophoresis, and electro transferred to polyvinylidene fluoride (PVDF) membranes. The PVDF membranes were blocked in blocking buffer for 2 h at RT, followed by incubation with the following antibodies overnight at 4 °C: mouse anti-β-actin (Proteintech, Wuhan, China, Cat# 66009-1-Ig, 1:1000 dilution), rabbit anti-ANGPTL8 (Thermo Fisher Scientific, MA, USA, Cat# PA5-38043, 1:1000 dilution), anti-ERK1/2 (Cell Signaling Technology, MA, USA, Cat# 4695T, 1:1000 dilution), anti-phospho-ERK1/2 (Thr202/Tyr204; Cell Signaling Technology, MA, USA, Cat# 4370T, 1:1000 dilution), anti-AKT (Cell Signaling Technology, MA, USA, Cat# 4691S, 1:1000 dilution), anti-phospho-AKT (Ser473; Cell Signaling Technology, MA, USA, Cat# 4060T, 1:1000 dilution), anti-ROCK (Abclonal, China, Cat# A2359, 1:1000 dilution), anti-Cofilin-1 (Abclonal, China, Cat# A1704, 1:1000 dilution), and anti-phospho-Cofilin-1 (Abclonal, China, Cat# AP0178, 1:1000 dilution). The blots were subsequently rinsed with Tris-buffered saline containing Tween-20 (TBST) three times and incubated with anti-rabbit peroxide-conjugated secondary antibodies for 90 min. The protein bands were visualized and detected using an enhanced chemiluminescence system.

Statistical analyses

For animal studies, mice were randomized by body weight prior to dietary challenge, and no blinding was performed for subsequent analyses. Statistical analyses were performed with Prism 7 (GraphPad Software, Inc., USA). For data with a normal distribution and homogeneity of variance, one-way or two-way ANOVA was performed for comparisons among more than two groups. Two-tailed Student's t tests were performed to evaluate significant differences between two groups. The statistical tests used for each experiment are indicated in the figure legends. All data are expressed as the mean ± s.e.m. unless otherwise indicated. $P < 0.05$ was considered statistically significant. All in vitro experiments were performed in triplicate. Animal feeding, treatments and histological analyses were performed in a single-blinded fashion. No blinding was used for the remaining analyses.

Results

ANGPTL8 levels were increased in the serum and CSF of patients and mice with diabetes-associated cognitive dysfunction

After completing the MMSE and MoCA scales, clinical participants were divided into three groups matched for sex, age, and body mass index (BMI): healthy control, diabetes without cognitive dysfunction, and diabetes with cognitive dysfunction (Supplementary Table 2). There was no significant difference in circulating ANGPTL8 levels regardless of whether the cognition of diabetic patients declined, although the levels were higher in diabetes patients (Fig. 1A). However, ANGPTL8 levels in the CSF of diabetes patients with cognitive dysfunction were higher than those in the CSF of patients without cognitive dysfunction (Fig. 1B).

Nine-month-HFD-fed mice and 6-month-ND-fed db/db mice, both diabetic mice marked by significantly elevated blood glucose levels and insulin resistance (sFig. 1C and D), were used to mimic the pathogenesis of diabetes-associated cognitive dysfunction. Significantly less distance traveled and velocity were observed in both diabetic mouse models than in controls in the open field test (sFig. 1E). The impaired cognitive function of both diabetic mouse models was confirmed by a decreased recognition index (Fig. 1C–F), but not general activity (sFig. 1F and G), in the novel object recognition test and increased errors in the Barnes maze compared with the control group (Fig. 1G–I). Similar to patients with diabetes-associated cognitive dysfunction, diabetic mice exhibited higher circulating and CSF ANGPTL8 levels relative to the control group (Fig. 1J and K). Moreover, ANGPTL8 levels were increased in the serum and CSF of STZ-induced diabetes model mice with diabetes-associated cognitive dysfunction (sFig. 2A–N).

Furthermore, the body weight of diabetic mice, HFD-fed mice and db/db mice, was higher than that of mice in the control groups (sFig. 1A), but this was not found in STZ-induced diabetes model mice (sFig. 2I). Moreover, diabetic mice exhibited obvious insulin resistance (sFig. 1C and D; sFig. 2K and L). No difference in lipids levels was observed between diabetic mice with diabetes-associated cognitive dysfunction and the control group (sFig. 1B; sFig. 2J).

ANGPTL8 expression was increased in the hippocampus of diabetic brains

Consistently, the mRNA expression of *Angptl8* was increased in the hippocampal tissue of diabetic mice with cognitive impairment (Fig. 1L; sFig. 2G), and intracellular

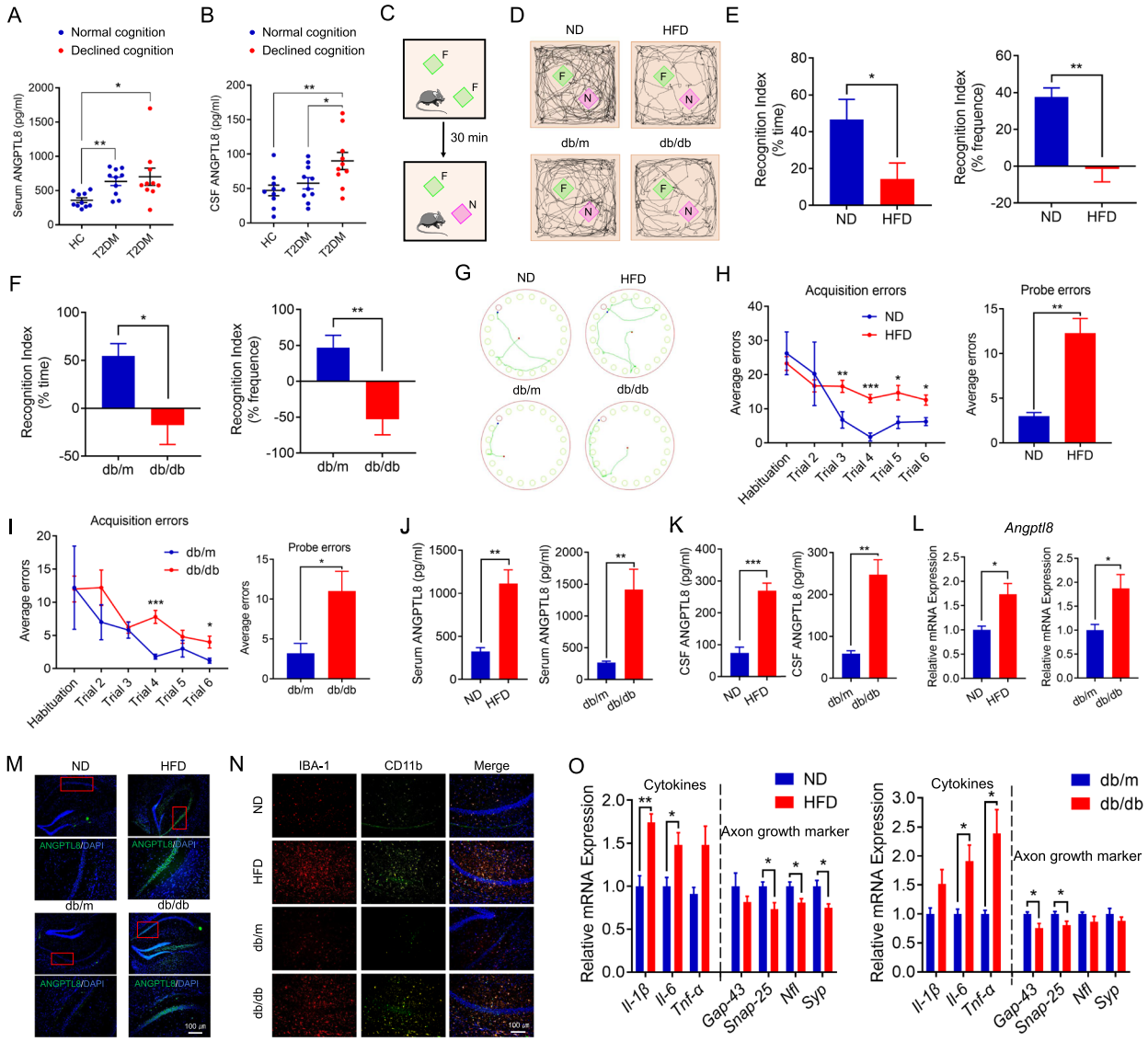

Fig. 1 ANGPTL8 levels were increased in the serum and CSF of patients and mice with diabetes-associated cognitive dysfunction. **A** Serum ANGPTL8 levels in the indicated groups (n = 10 per group). **B** ANGPTL8 levels in the CSF of the indicated groups (n = 10 per group). **C** Schematic depicting the novel object recognition task (the green square represents the familiar object, and the purple square represents the novel object). F, familiar object; N, novel object. **D** Representative traces of paths by the indicated mice to explore novel objects. **E**, **F** Recognition index of the indicated mice, calculated as the difference in the amount of time spent exploring the novel and familiar objects (left) and in the frequency of novel object explorations and familiar object explorations (right) (n = 4–7 mice per group). **G** Representative traces of paths to the target hole (red) by the indicated mice on the day of testing in the Barnes maze. **H**, **I** Barnes maze acquisition and probe trials for the indicated mice, shown by average errors. **J** Serum ANGPTL8 levels in the indicated groups. **K** CSF ANGPTL8 levels in the indicated groups. **L** *Angptl8* mRNA expression in the hippocampus in the indicated groups. **M** Immunofluorescence analysis of ANGPTL8 protein expression in the hippocampal CA1 region of the indicated mice. **N** Immunofluorescence staining of IBA-1 (red) and CD11b (green) in the hippocampal CA1 region of the indicated mice. **O** mRNA expression of proinflammatory cytokines (*Il-1β*, *Il-6*, and *Tnf-α*) and axonal growth and synaptic plasticity markers (*Gap-43*, *Snap-25*, *Nfl*, and *Syp*) in the hippocampus of the indicated groups. The data are shown as the mean ± s.e.m. and were statistically analyzed by two-way ANOVA with Bonferroni's test (**A**, **B**) and two-tailed Student's t test (**C**–**O**). *$P < 0.05$, **$P < 0.01$, ***$P < 0.001$, ****$P < 0.0001$. NS: nonsignificant. CSF: cerebrospinal fluid; HC: healthy control; T2DM: type 2 diabetes mellitus

ANGPTL8 protein expression in diabetic brain tissue was visualized by immunofluorescence of tissue sections (Fig. 1M). Further analysis revealed that diabetic mice with impaired cognitive function exhibited more microglia (marked by IBA-1) infiltrating the hippocampal CA1 region (Fig. 1N) as well as higher inflammatory

markers (CD11b and CD16/32) and fewer anti-inflammatory markers (CD206) (Fig. 1N; sFig. 1H). Moreover, the mRNA expression of proinflammatory cytokines (*Il-1β*, *Il-6*, and *Tnf-α)* (Fig. 1O; sFig. 2H) was increased in the hippocampal tissue of diabetic mice with cognitive impairment, while the mRNA expression of the axonal growth and synaptic plasticity markers growth-associated protein-43 (*Gap-43*), synaptosomal-associated protein 25 (*Snap-25*), neurofilament light chain (*Nfl*) and synaptophysin (*Syp*), which play vital roles in many neuronal functions, including axonal growth and the expression of long-term potentiation (LTP), in the hippocampus [36–44] was decreased (Fig. 1O; sFig. 2H). The results indicated that diabetic mice exhibited obvious neuroinflammation, decreased growth of neuronal axons, and damaged synapses in the hippocampus.

ANGPTL8 derived from neurons in the diabetic brain

It was unclear whether the increased ANGPTL8 levels in CSF were due to more circulating ANGPTL8 crossing the blood–brain barrier or increased production from brain tissue. Purified flag-targeted ANGPTL8 protein (rA8-flag) was injected peripherally and was not detected in brain tissues (sFig. 3A). Furthermore, LPS was injected intraperitoneally, and *Angptl8* expression was upregulated in the hippocampus (sFig. 3B and C). Moreover, an in vitro study showed that the mRNA expression of *Angptl8* was also increased in hippocampal neurons but not microglia when treated with LPS or TNF-α (sFig. 3D and E), indicating that increased ANGPTL8 in brain tissue mainly originated from neural cells rather than microglia. Furthermore, the mRNA expression of *Angptl8* was also increased in hippocampal neurons but not microglia after exposure to high glucose levels (sFig. 2O). Based on the above observation, the increased levels of ANGPTL8 protein in diabetic CSF probably originated directly from brain tissue rather than from circulation.

Depletion of *Angptl8* in the CNS protected against diabetes-associated cognitive dysfunction and alleviated neuroinflammation

Given the association between neuroinflammation and cognitive impairment, we reasoned that a reduction in neuronal ANGPTL8 levels and the consequent alleviation of inflammation and synaptic injury might protect cognitive function in diabetic mice. Considering that ANGPTL8 in the CNS was mainly expressed on neurons independent of circulating ANGPTL8, we crossed Nestin-Cre mice (broadly used for selective gene deletion in neurons of the CNS [45]) with floxed *Angptl8* transgenic mice to generate neuronal *Angptl8* cKO mice (referred to as *Angptl8*^{Nestin} *CKO*) to study the function of neuronal ANGPTL8 in vivo (Fig. 2A). *Angptl8* CKO was confirmed by the fact that neuronal ANGPTL8 expression was significantly eliminated in the hippocampus (Fig. 2C and D) and that ANGPTL8 was undetectable in the CSF (Fig. 2B). We next examined whether the conditional deletion of *Angptl8* in neurons affected hippocampal development and cognitive function. As shown in Fig. 2E, F and Fig. 3A, there was no significant difference in body weight (Fig. 3A), neuronal number or neuronal distribution in the hippocampus (Fig. 2E and F) between *Loxp/loxp* and *Angptl8*^{Nestin} *CKO* mice. Moreover, we found that conditional deletion of *Angptl8* in neurons did not affect the cognitive function of normal diet-fed mice based on behavior tests including the open field test (sFig. 4A), novel object recognition test and Barnes maze test (Fig. 2G–J). Taken together, these results indicated that conditional deletion of *Angptl8* in neurons did not affect the development of neurons or cognitive function. Furthermore, depletion of *Angptl8* in the CNS did not affect body weight (Fig. 3A) and levels of glucose (Fig. 3B–E) or lipids (Fig. 3F) in mice fed an ND or HFD.

Similar to the results shown in Fig. 1, mice fed an HFD for 9 months exhibited higher CSF ANGPTL8 levels than ND-fed mice in *Loxp/loxp* group but not *Angptl8*^{Nestin} *CKO* group mice (Fig. 2B). Blood glucose levels and insulin resistance were also significantly elevated in mice fed an HFD compared to ND-fed mice, but there was no difference between *Loxp/loxp* and *Angptl8*^{Nestin} *CKO* mice regardless of whether they were fed an HFD (Fig. 3B–E). Significantly less distance traveled and velocity were observed in 9-month-HFD-fed mice than in controls in the open field test (sFig. 4A). Hippocampus-dependent spatial memory is particularly vulnerable to diabetes-associated cognitive dysfunction, so the performance of mice in the new object recognition test and the Barnes maze task was tested. The cognitive function of *Loxp/loxp* mice fed an HFD for 9 months was impaired, as compared with control mice, they exhibited decreases in recognition index (Fig. 2G and H), but not general activity (sFig. 4B), in the novel object recognition test; an increased number of errors in the Barnes maze (Fig. 2I and J); more microglia (marked by IBA-1) infiltrating the hippocampal CA1 region (Fig. 3G); higher levels of inflammatory markers (CD11b and CD16/32) (Fig. 3G and H); fewer synapses (Fig. 3I and J); and more swollen postsynaptic membranes, blurred synaptic sites or missing synaptic sites (Fig. 3I); upregulation of inflammatory cytokine mRNA expression (*Il-1β*, *Il-6*, and *Tnf-α*); and decreased expression of axonal growth and synaptic plasticity markers (*Gap-43*, *Snap-25*, *Nfl*, and *Syp*) (Fig. 3K).

Notably, we observed that compared with ND-fed *Angptl8*^{Nestin} *CKO* mice, HFD-fed *Angptl8*^{Nestin} *CKO* mice exhibited no obvious changes. In both tasks, *Angptl8*^{Nestin}

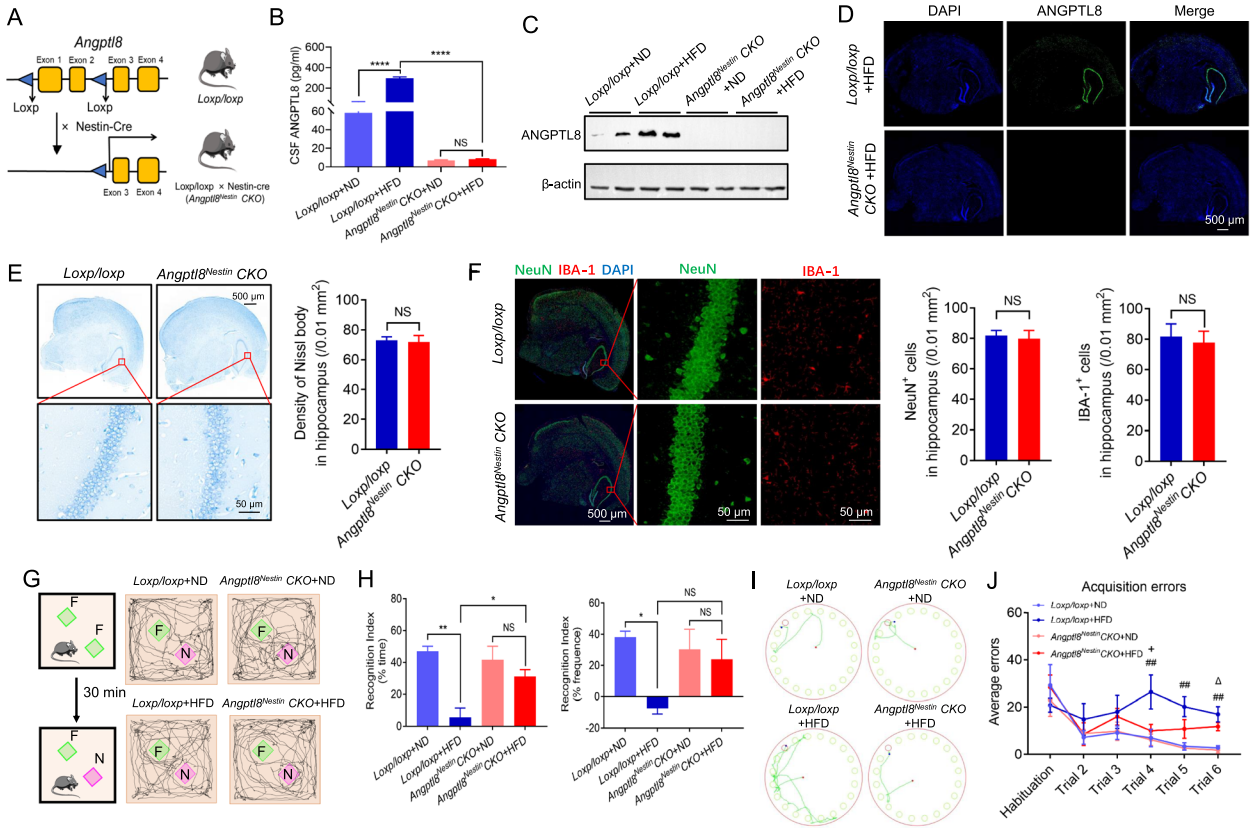

Fig. 2 Depletion of *Angptl8* in the central nervous system (CNS) protected against diabetes-associated cognitive dysfunction. **A** Strategy used to generate *Angptl8*^{Nestin} CKO mice. **B** ANGPTL8 levels in CSF in the indicated groups (n = 5 mice per group). **C** Western blotting analysis of ANGPTL8 in the brain tissue of the indicated mice. **D** Immunofluorescence staining showing *Angptl8* knockout efficiency in the hippocampus of HFD-fed *Angptl8* conditional knockout (CKO) mice. **E** Nissl staining images showing Nissl bodies in the hippocampus of male *Loxp/loxp* and *Angptl8*^{Nestin} *CKO* mice (left). Quantitative analysis of the number of neurons (right) (n = 5 per group). **F** Double immunostaining of NeuN (green) and IBA-1 (red) in the hippocampus of male *Loxp/loxp* and *Angptl8*^{Nestin} *CKO* mice (left). Quantitative analysis of the number of NeuN + and IBA-1 + cells (right) (n = 5 per group). **G** Representative traces of paths by the indicated mice to explore a novel object (the green square represents the familiar object, and the purple square represents the novel object). F, familiar object; N, novel object. **H** Recognition index of the indicated mice (n = 5 mice per group), calculated as the difference in the amount of time spent exploring the novel and familiar objects (left) and in the frequency of novel object explorations and familiar object explorations (right). **I** Traces of paths to the target hole (red) in Barnes maze probe trials for the indicated mice. **J** Barnes maze acquisition and probe trials for the indicated groups (n = 5 mice per group). **P* < 0.05, ***P* < 0.01, *****P* < 0.0001; + *P* < 0.05: *Loxp/loxp* + HFD group vs. *Angptl8*^{Nestin} *CKO* + HFD group; ##*P* < 0.01: *Loxp/loxp* + ND group vs. *Loxp/loxp* + HFD group; Δ*P* < 0.05: *Angptl8*^{Nestin} *CKO* + ND group vs. *Angptl8*^{Nestin} *CKO* + HFD group. NS, nonsignificant. The data are shown as the mean ± s.e.m. and were statistically analyzed by two-way ANOVA with Bonferroni's test. CSF: cerebrospinal fluid

CKO mice fed an HFD for 9 months exhibited better cognitive function than their *floxed* littermates (as controls), as evidenced by a higher recognition index for the novel objects (Fig. 2G and H), not general activity (sFig. 4B), and fewer errors in the Barnes maze test (Fig. 2I and J). Thus, a reduction in neuronal ANGPTL8 expression in diabetic mice protects hippocampus-mediated memory.

Moreover, the 9-month-HFD-fed *Angptl8*^{Nestin} *CKO* mice exhibited fewer microglia (marked by IBA-1) infiltrating the hippocampal CA1 region (Fig. 3G), fewer inflammatory markers (CD16/32 and CD11b) and more anti-inflammatory markers (CD206) (Fig. 3H). Next, we assessed the synaptic integrity of hippocampal neurons by electron microscopy analysis (Fig. 3I). Compared with 9-month-HFD-fed *floxed* mice, 9-month-HFD-fed *Angptl8*^{Nestin} *CKO* mice showed increases in synapse number (Fig. 3I and J). In higher magnification images of brain slices of *Angptl8*^{Nestin} *CKO* mice, we also observed that the presynaptic and postsynaptic membranes were clear and had complete outlines, and the synaptic cleft was evident (Fig. 3I). Similarly, decreased neuroinflammation and increased synaptic connectivity were observed in the hippocampal tissue of *Angptl8*^{Nestin} *CKO* mice, as shown by decreased expression of inflammatory

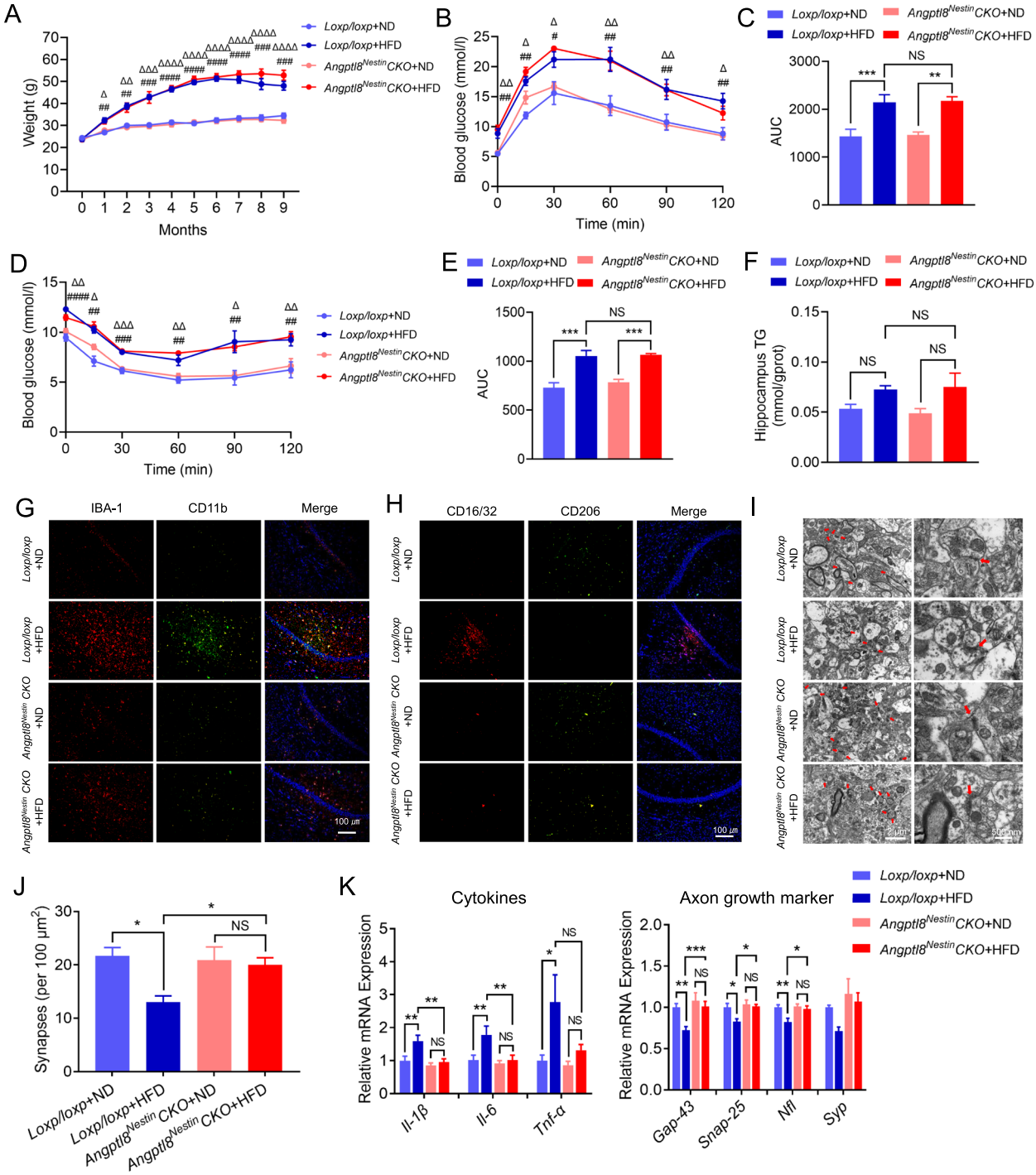

Fig. 3 Depletion of *Angptl8* in the CNS protected against synaptic damage and alleviated neuroinflammation. **A** Body weight of the indicated mice. **B**, **C** GTT and area-under-the-curve (AUC) values of the indicated mice. **D**, **E** ITT and AUC values of the indicated mice. **F** Hippocampal TG levels of the indicated mice. **G** Immunofluorescence staining of IBA-1 (red) and CD11b (green) in the CA1 region of the hippocampus in the indicated mice. **H** Immunofluorescence staining of CD16/32 (red) and CD206 (green) in the hippocampal CA1 region in the indicated mice. **I** Representative images of synaptic ultrastructure (red arrow) in the hippocampus. **J** Quantification of the number of synapses in the indicated mice. **K** mRNA expression of proinflammatory cytokines (*Il-1β*, *Il-6*, and *Tnf-α*) and axon growth and synaptic plasticity markers (*Gap-43*, *Snap-25*, *Nfl*, and *Syp*) in the hippocampus of the indicated groups (n = 5 mice per group). **P* < 0.05, ***P* < 0.01, ****P* < 0.001; #*P* < 0.05, ##*P* < 0.01, ###*P* < 0.001, ####*P* < 0.0001: *Loxp/loxp* + ND group vs *Loxp/loxp* + HFD group; Δ*P* < 0.05, ΔΔ*P* < 0.01, ΔΔΔ*P* < 0.001, ΔΔΔΔ*P* < 0.0001: *Angptl8*^{Nestin} *CKO* + ND group vs *Angptl8*^{Nestin} *CKO* + HFD group. NS: nonsignificant. The data are shown as the mean ± s.e.m. and were statistically analyzed by two-way ANOVA with Bonferroni's test

cytokines (*Il-1β*, *Il-6*, and *Tnf-α*) and increased expression of axonal growth and synaptic plasticity markers (*Gap-43*, *Snap-25*, *Nfl*, and *Syp*) (Fig. 3K).

Moreover, to exclude the off-target effects of Nesting-Cre, AAV-Nestin-Cre was directly injected into the hippocampus of diabetic *floxed* mice fed an HFD for 6 months (sFig. 5A and B). After HFD feeding for an additional 3 months, AAV-Cre + HFD mice exhibited improved cognitive function (sFig. 5C-F), improved synaptic structure (sFig. 5H-J), and alleviated neuroinflammation (sFig. 5G and J; sFig. 6G) in comparison to AAV-Control + HFD group mice, with no discernible effects on body weight (sFig. 6A), glucose (sFig. 6C and D) or lipid (sFig. 6B) metabolism, or general activity (sFig. 6E and F).

ANGPTL8 induced synaptic injury and neuroinflammation

In our previous study, GST pulldown assays confirmed ANGPTL8-PirB binding [15]. In light of the immunofluorescence colocalization of ANGPTL8 and PirB in the hippocampal CA1 region (Fig. 4A), we isolated and cultured primary hippocampal cells to identify the potential cellular location of ANGPTL8-PirB in the hippocampus. We observed that rA8-flag colocalized with PirB on neurons and microglia cells (Fig. 4B) but not astrocytes or endothelial cells (data not shown). Given that ANGPTL8 is a secreted hormone and is unable to penetrate the cell membrane, we speculated that PirB is the receptor for ANGPTL8 on neurons and microglia cells. To identify the potential functions of ANGPTL8 in neurons, we further analyzed ANGPTL8-inducced changes in the transcriptional profile of neurons through mRNA sequencing. Pathway enrichment analysis revealed that the upregulated genes in neurons after ANGPTL8 treatment were enriched in pathways associated with axonal injury (Fig. 4C). Markers of axonal growth and synaptic plasticity were downregulated after ANGPTL8 treatment (Fig. 4D). Based on the above analysis, the effects of ANGPTL8 in neurons were further analyzed. We found that ANGPTL8 significantly inhibited axonal growth, reduced synaptic connectivity (Fig. 4E), and downregulated the mRNA expression of axonal growth and synaptic plasticity markers (*Gap-43*, *Snap-25*, *Nfl*, and *Syp*) in a dose-dependent manner (Fig. 4F). In addition, we analyzed transcriptional changes in microglia and found that M1 (inflammatory phenotype) marker genes were highly upregulated after ANGPTL8 treatment (Fig. 4G). Consequently, we referred to CD11b as an M1 marker and CD206 as an M2 (anti-inflammatory phenotype) marker with IBA-1 costaining to identify the polarization of microglia by flow cytometry. After ANGPTL8 stimulation, the CD11b + population was increased, whereas the CD206 + population was decreased (Fig. 4H). Taken together, these results suggest that ANGPTL8 is a proinflammatory protein resulting in aggravated synaptic injury and microglial M1-type polarization.

PirB mediated ANGPTL8-induced synaptic injury and neuroinflammation

PirB is a receptor with an intracellular domain recruiting phosphatases to dephosphorylate downstream signals [46]. Therefore, we measured the phosphorylation of signals downstream of PirB in neurons and microglia. Induced by ANGPTL8 stimulation, primary neurons exhibited activated phosphorylation levels of the PirB downstream proteins AKT and ERK, leading to upregulation of ROCK2 protein expression (a neurite growth-inhibiting factor [47]) and inhibiting downstream cofilin protein phosphorylation (Fig. 5A and B). Consistent with neurons, microglia also exhibited increased phosphorylation levels of AKT, ERK, P38 and P65 after stimulation with ANGPTL8 (Fig. 5G). To investigate whether the activated signals were specifically mediated by the ANGPTL8-PirB axis, a PirB blockade assay was performed on neurons and microglia. ANGPTL8-induced inhibition of neuronal axon growth and microglial proinflammatory polarization were abrogated in the PirB blockade group compared to control group, as evidenced by increased expression of axonal growth and synaptic plasticity markers (*Gap-43*, *Snap-25*, *Nfl*, and *Syp*) (Fig. 5C), ameliorated synaptic connectivity (Fig. 5D), and downregulation of M1 markers (*Il-1β*, *Il-6*, and *Tnf-α*) (Fig. 5H). To further evaluate the underlying mechanisms, we used small-molecule inhibitors to suppress the phosphorylation of signals downstream of PirB (AKT, ERK, P38, and P65). The results showed that inhibiting the phosphorylation of ERK1/2 (U0126) attenuated ANGPTL8-induced suppression of axonal growth and synaptic connectivity, whereas inhibitors of p-AKT (MK-2206) failed to produce the same results (Fig. 5E and F). In contrast, inhibitors of p-P38 (SB203580) and p-P65 (BAY 11-7082), but not p-AKT or p-ERK1/2, abrogated the ANGPTL8-induced production of proinflammatory cytokines in microglia (Fig. 5I). These data suggested that ANGPTL8-induced neuronal injury was predominantly mediated by the ERK1/2 signaling pathway, whereas the proinflammatory polarization of microglia was mediated by the P38 and P65 signaling pathways.

PirB$^{-/-}$ mice were resistant to ANGPTL8-induced neuroinflammation and synaptic injury

To assess whether ANGPTL8 exerts proinflammatory and synapse-damaging effects via PirB in vivo, we injected exogenous ANGPTL8 into the hippocampus of WT mice and *PirB*$^{-/-}$ mice for 30 days (Fig. 6A). There was no significant difference in body weight

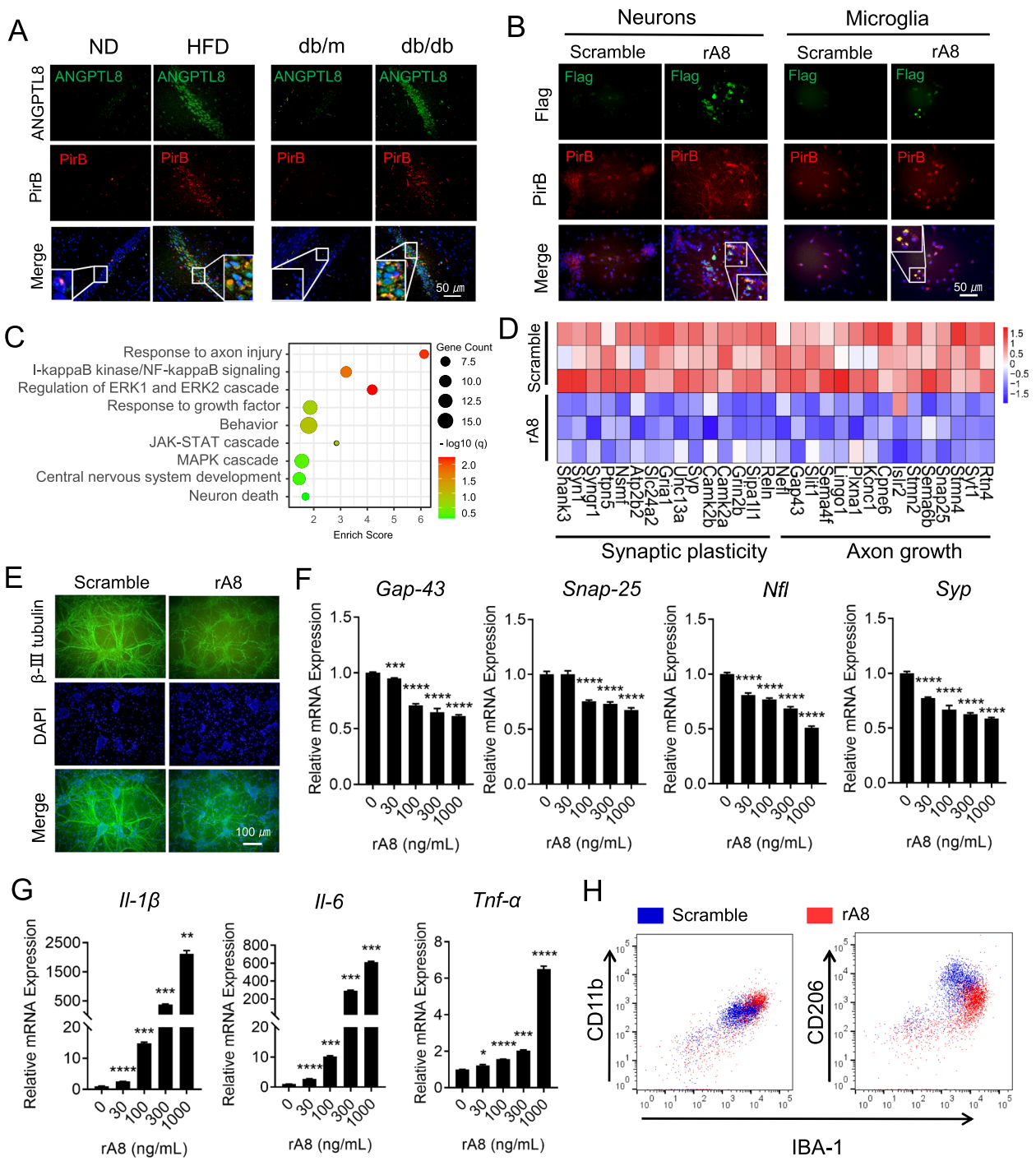

Fig. 4 ANGPTL8 induced synaptic injury and neuroinflammation. **A** Immunofluorescence analysis of ANGPTL8 and PirB in the hippocampal CA1 region of the indicated mice. **B** Immunofluorescence analysis of colocalization of ANGPTL8 and PirB in mouse neurons and microglia. **C** Pathway enrichment analysis of neurons treated with rA8. **D** Heatmap showing differences in relative mRNA expression in neurons treated with scramble or rA8. **E** Immunofluorescence staining of β-III tubulin (green) in neurons treated with scrambled ANGPTL8 or rA8 (1000 ng/ml). **F** mRNA expression of axonal growth and synaptic plasticity markers in neurons treated with different concentrations of rA8 for 5 days (n = 6). Comparisons were performed between untreated groups and treated groups. **G** mRNA expression of proinflammatory cytokines in microglia treated with different concentrations of rA8 for 24 h (n = 3). Comparisons were performed between untreated groups and treated groups. **H** Flow cytometry of microglial polarization after treatment with scrambled ANGPTL8 or rA8 (1000 ng/ml). *$P < 0.05$, **$P < 0.01$, ***$P < 0.001$, ****$P < 0.0001$. The data are shown as the mean ± s.e.m. and were statistically analyzed by one-way ANOVA with Bonferroni's test. rA8: flag-targeted recombinant ANGPTL8 protein

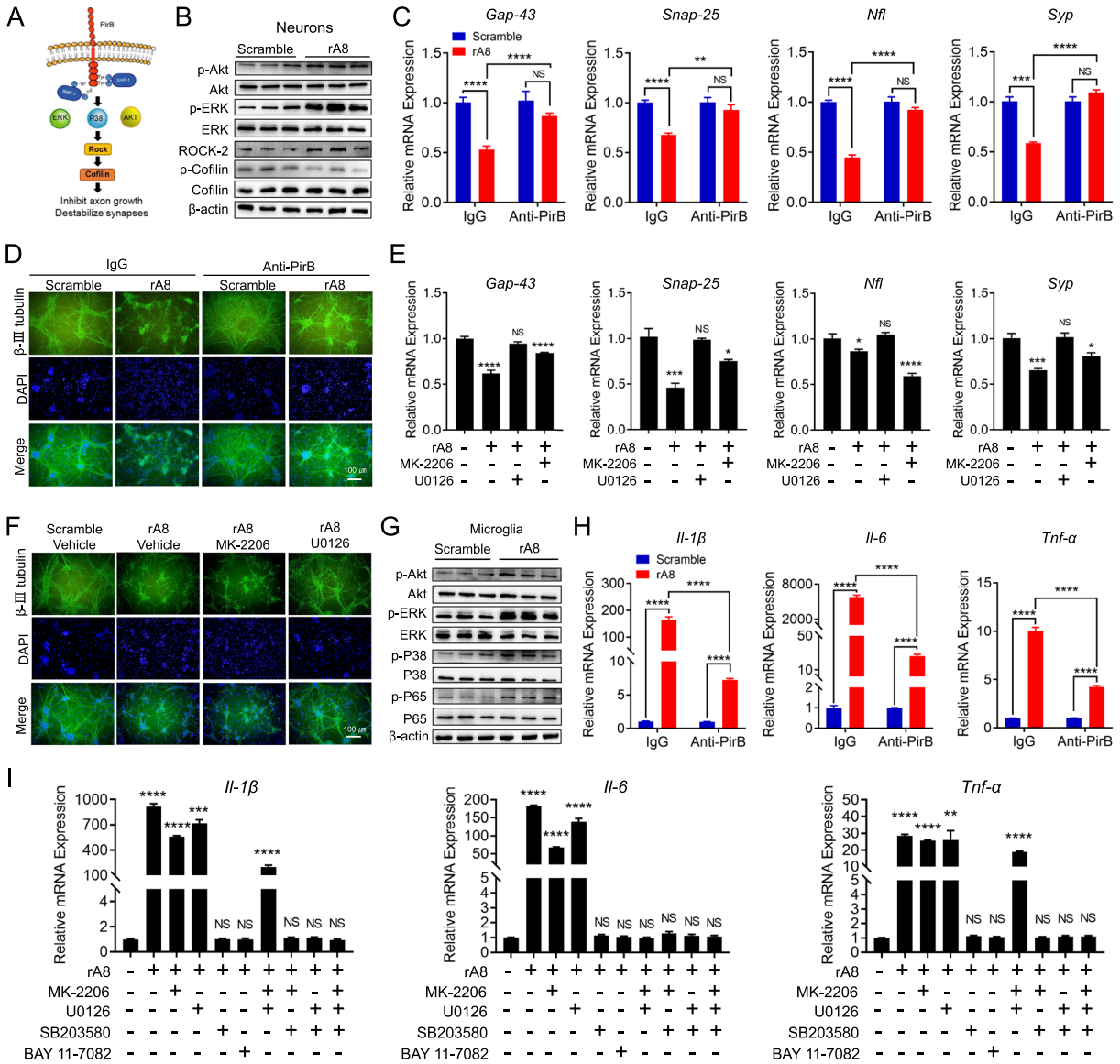

Fig. 5 PirB mediated ANGPTL8-induced synaptic injury and neuroinflammation. **A** Scheme showing the signaling pathway downstream of PirB as indicated in the literature. **B** Western blot showing the phosphorylation of AKT, ERK1/2, ROCK2, and Cofilin in mouse neurons stimulated with scrambled ANGPTL8 or rA8 (1000 ng/ml). **C** mRNA expression of axonal growth and synaptic plasticity markers (*Gap-43*, *Snap-25*, *Nfl*, and *Syp*) in mouse neurons pretreated with the indicated antibodies before rA8 stimulation (n = 6). **D** Immunofluorescence staining showing the synaptic connections of neurons treated with the indicated conditions. **E** mRNA expression of axonal growth and synaptic plasticity markers (*Gap-43*, *Snap-25*, *Nfl*, and *Syp*) in mouse neurons treated by the indicated conditions (n = 6). Comparisons were performed between untreated groups and treated groups. **F** Immunofluorescence staining showing the synaptic connections of neurons treated with the indicated conditions. **G** Western blot analysis of the phosphorylation of signaling molecules in mouse microglia stimulated with scrambled ANGPTL8 or rA8 (1000 ng/ml). **H** mRNA expression of proinflammatory cytokines in mouse microglia cells pretreated with control IgG or an anti-PirB ectodomain antibody for 30 min followed by 24-h stimulation with scrambled ANGPTL8 or rA8 (1000 ng/ml) (n = 6). **I** mRNA expression of proinflammatory cytokines in mouse microglia treated with the indicated conditions (n = 6). Comparisons were performed between untreated groups and treated groups. The data are shown as the mean ± s.e.m. and were statistically analyzed by two-tailed Student's t test (**C**, **H**) or one-way ANOVA with Bonferroni's test (**E**, **I**). *$P < 0.05$, **$P < 0.01$, ***$P < 0.001$, ****$P < 0.0001$. NS: nonsignificant; rA8: flag-targeted recombinant ANGPTL8 protein; MK-2206: p-AKT inhibitor; U0126: p-ERK1/2 inhibitor; SB203580: p-P38 inhibitor; BAY11-7082: p-P65 inhibitor

(sFig. 7A), glucose (sFig. 7C and D), or lipids (sFig. 7B) levels between WT mice and *PirB*$^{-/-}$ mice after injection of exogenous ANGPTL8 into the hippocampus. Moreover, no significant difference was observed between ANGPTL8 protein-treated mice and controls in distance traveled or velocity (sFig. 7E). Compared

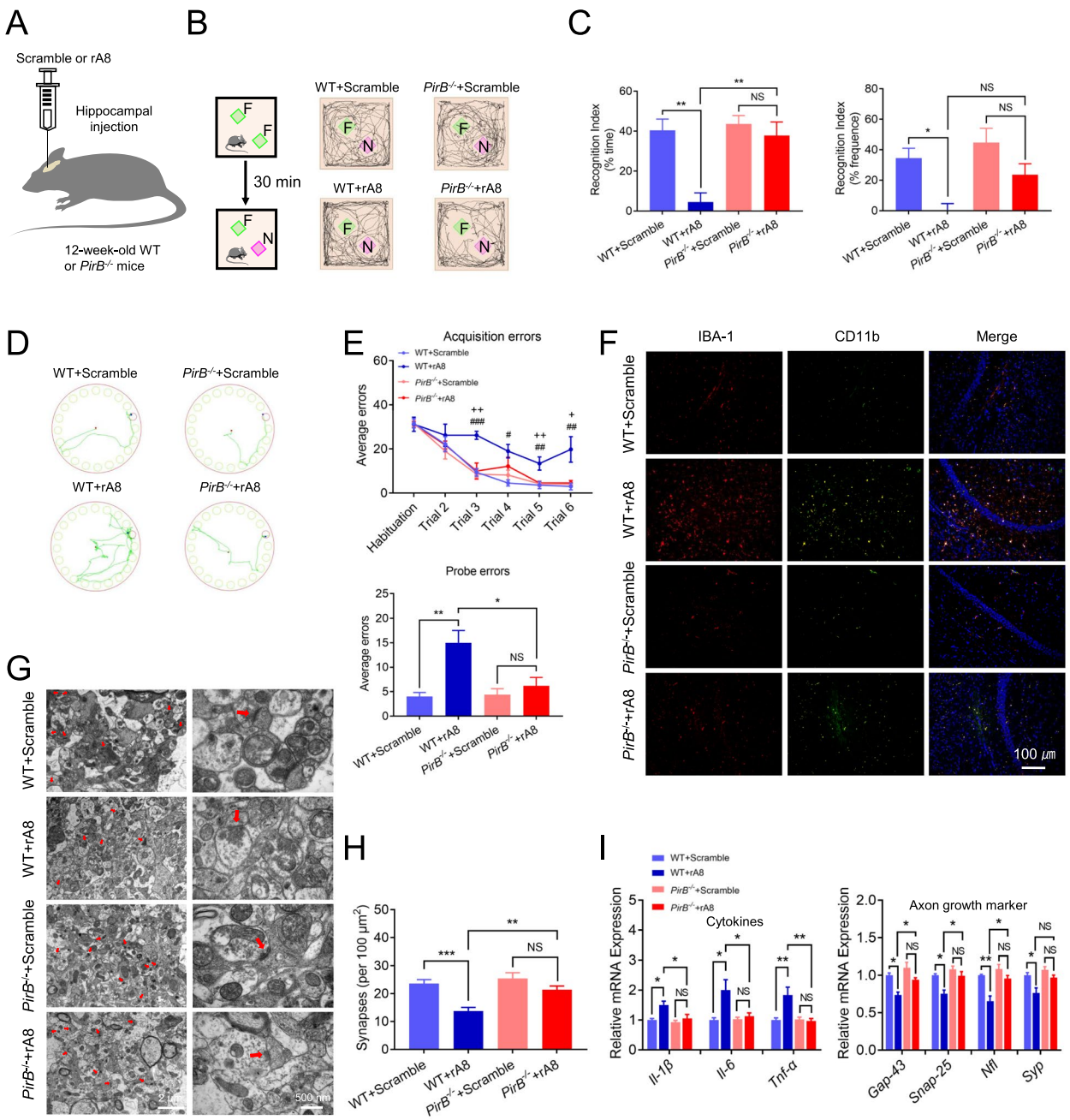

Fig. 6 *PirB*$^{-/-}$ mice were resistant to ANGPTL8-induced neuroinflammation and synaptic injury. **A** Experimental scheme. **B** Representative traces of paths by the indicated mice to explore a novel object (the green square represents the familiar object, and the purple square represents the novel object). F, familiar object; N, novel object. **C** Recognition index of the indicated mice (n = 5 mice per group), calculated as the difference in the amount of time spent exploring the novel and familiar objects (left) and in the frequency of novel object explorations and familiar object explorations (right). **D** Traces of paths to the target hole (red) in Barnes maze probe trials for the indicated mice. **E** Barnes maze acquisition and probe trials for the indicated groups (n = 5 mice per group). **F** Immunofluorescence staining of IBA-1 (red) and CD11b (green) in the hippocampal CA1 region of the indicated mice. **G** Representative images of synaptic ultrastructure (red arrow) in the hippocampus of the indicated mice. **H** Quantification of the number of synapses in the hippocampus of the indicated mice. **I** mRNA expression of proinflammatory cytokines (*Il-1β*, *Il-6*, and *Tnf-α*) and axonal growth and synaptic plasticity markers (*Gap-43*, *Snap-25*, *Nfl*, and *Syp*) in the hippocampus of the indicated groups. *$P < 0.05$, **$P < 0.01$, ***$P < 0.001$; +$P < 0.05$, ++$P < 0.01$: WT + rA8 group vs. *PirB*$^{-/-}$ + rA8 group; #$P < 0.05$, ##$P < 0.01$, ###$P < 0.001$: WT + Scrambled group vs. WT + rA8 group. NS, nonsignificant. The data are shown as the mean ± s.e.m. (n = 5 mice per group) and were statistically analyzed by two-way ANOVA with Bonferroni's test. rA8, flag-targeted recombinant ANGPTL8 protein

with those injected with the control protein, WT mice injected with the ANGPTL8 protein exhibited a lower recognition index for the novel objects (Fig. 6B and C) but not lower general activity (sFig. 7F); more errors in the Barnes maze test (Fig. 6D and E); more microglia (marked by IBA-1) infiltrating the hippocampal CA1 region (Fig. 6F); higher levels of inflammatory markers (CD11b and CD16/32) (Fig. 6F; sFig. 7G); fewer synapses (Fig. 6G and H); more swollen postsynaptic membranes, blurred synaptic sites or missing synaptic sites (Fig. 6G); upregulation of inflammatory cytokine mRNA expression (*Il-1β*, *Il-6*, and *Tnf-α*); and decreased expression of axonal growth and synaptic plasticity markers (*Gap-43*, *Snap-25*, *Nfl*, and *Syp*) (Fig. 6I). Notably, we observed that $PirB^{-/-}$ mice had no obvious changes after ANGPTL8 injection relative to the control group (Fig. 6B–I), indicating that $PirB^{-/-}$ mice were resistant to ANGPTL8-induced neuroinflammation and synaptic injury.

Discussion

In diabetes-associated cognitive dysfunction, the hippocampus is characterized by damaged neuronal axons and synapses and elevated proinflammatory cytokines [48]. In the present study, elevated ANGPTL8 levels were found in the hippocampus and CSF of mouse models with diabetes-associated cognitive dysfunction, which bind with their receptor (PirB) on neurons and microglia to trigger neuronal damage and neuroinflammation through the PirB-mediated signaling pathway, indicating that ANGPTL8 directly causes the impairment of neurons (Fig. 7).

We and others have found elevated levels of circulating ANGPTL8 in individuals with diabetes [11, 49]. The present study revealed that ANGPTL8 levels increased not only in the circulation but also in the CSF of those afflicted by diabetes-associated cognitive dysfunction. These results indicate that ANGPTL8 may induce cognitive impairment in patients with diabetes. Among patients with type 2 diabetes, not difference for BMI, HbA1c, fasting blood glucose, and TG levels in those with and without cognitive decline, suggests that increased ANGPTL8 expression in the CSF of diabetic patients with cognitive decline was not associated with body weight or blood glucose levels. Recent studies on diabetes-associated cognitive dysfunction have shown that the development of cognitive dysfunction may be related to brain insulin resistance, persistent low-grade inflammation [50]. Therefore, we speculate that the elevation of ANGPTL8 levels in the brain may be related to these factors, as ANGPTL8 is one of important inflammatory factors [15, 51].

Our study also found that ANGPTL8 in the CSF was derived from brain tissue rather than crossing via the blood–brain barrier from circulation. Chronic low-grade inflammation, which occurs in diabetic conditions [24, 52], leads to ANGPTL8 production in the CA1 region of the hippocampus, where more microglial aggregation is detected in diabetic mice. In addition to the above reasons, insulin resistance may also contribute to increased ANGPTL8 production in brain tissue. It has been reported that insulin resistance occurs in the brain in individuals with diabetes and cognitive impairment [50] and causes increased production of ANGPTL8 [15, 53]. In this study, ANGPTL8 levels in the brain increased regardless of weight gain in diabetic mice. Therefore, factors other than obesity, such as neuroinflammation, brain insulin resistance, and a high glucose environment in the brain, may be the main inducers for the increased ANGPTL8 levels.

The present study also showed that depletion of *Angptl8* in the CNS prevented microglial infiltration, protected neurons from damage, and protected cognitive function. Moreover, no statistically significant difference was observed in neural development, body weight, GTT, ITT, or hippocampal TG levels between mice with depletion of *Angptl8* in the CNS and their control littermates following ND or HFD feeding. These results indicate that increased ANGPTL8 levels in the hippocampus rather than other factors are important for the occurrence of diabetes-related neuroinflammation and cognitive dysfunction. This is consistent with our previous study showing that hepatocyte-specific Angptl8 depletion reduced hepatic inflammation [15]. This finding provides ANGPTL8 as an innovative mechanism for diabetes-associated cognitive dysfunction.

PirB, a receptor expressed in neurons, is recognized for its role in inhibiting neurite outgrowth and impacting nervous system plasticity [54, 55]. In our previous studies, it was found that ANGPTL8 interacts with PirB on macrophages [15]. This is also consistent with recent findings highlighting that ANGPTL8 binds to PirB on cardiac cells and hepatocytes [56, 57]. In this study, we identified the colocalization of ANGPTL8 and PirB in both neurons and microglia. Notably, previous studies have demonstrated that PirB is involved in cognitive dysfunction through its modulation of axon outgrowth and synaptic plasticity [17, 26].

Considering that local secretion and diffusion of cells result in a concentration gradient of secreted proteins around the cell [58], protein concentrations in the CSF or plasma does not accurately reflect protein concentrations in extracellular fluids [59]. Since the actual ANGPTL8 concentration in the extracellular fluids of the CNS was unclear, we conducted concentration gradients to observe the effects of different ANGPTL8 concentrations, which was consistent with the previous

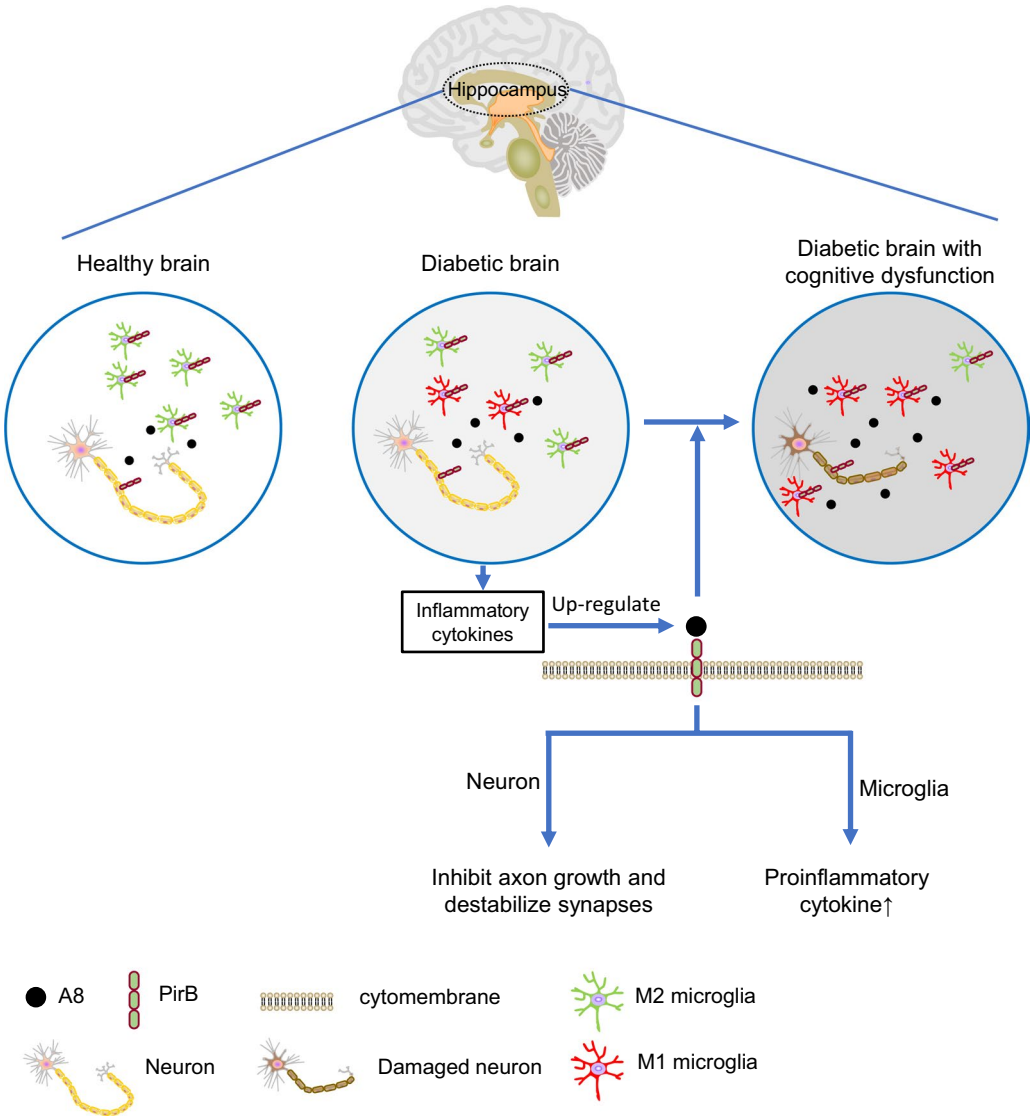

Fig. 7 Schematic showing that ANGPTL8 exaggerates diabetes-associated cognitive dysfunction by interacting with PirB on microglia and neurons. ANGPTL8 expression is increased along with decreased expression of synaptic and axonal markers and increased expression of proinflammatory cytokines in the hippocampus of diabetic brains with cognitive dysfunction. The colocalization of ANGPTL8 and paired immunoglobulin-like receptor B (PirB) on the surface of neurons and microglia membranes downregulates synaptic and axonal markers of neurons and upregulates the expression of proinflammatory cytokines in microglia, which reveals the role of ANGPTL8 in the pathogenesis of diabetes-associated cognitive dysfunction and identifies the ANGPTL8-PirB signaling pathway as a potential target for the management or treatment of diabetes-associated cognitive dysfunction

studies [56]. The results of mRNA sequencing revealed that ANGPTL8 contributed to axonal injury. The present study further provided evidence that PirB mediated the actions of ANGPTL8 in inhibiting axonal growth, reducing synaptic connectivity, and diminishing the expression levels of axonal growth and synaptic plasticity markers (*Gap-43*, *Snap-25*, *Syp*, and *Nfl*) in hippocampal neurons. These results are consistent with prior research, which has shown that PirB is related to reduced axon growth markers in neurodegenerative disease [26, 37, 39].

Moreover, this study delved into the role of ANGPTL8 in CNS inflammation. We found a substantial upregulation of M1 markers in microglia after ANGPTL8 treatment, accompanied by an increased M1 population and a decreased M2 population. Given the pivotal role of microglia-mediated inflammation in diabetes-associated cognitive dysfunction [60], this

finding implies that ANGPTL8, as a proinflammatory factor secreted from neurons and deposited in the hippocampus of the diabetic brain, may act in parallel to neurons and microglia in injuring synaptic plasticity, promoting neuroinflammation, and impairing cognitive performance and is thus involved in the development of diabetes-associated cognitive dysfunction. These results support the viewpoint that ANGPTL8 acts as a proinflammatory factor in pathologic conditions [15, 51, 61, 62].

For the molecular mechanisms underlying neuronal damage induced by ANGPTL8, primary neurons exhibited activated signaling pathways (AKT and ERK) downstream from PirB after ANGPTL8 stimulation, subsequently leading to the activation of ROCK2 signaling, of which upregulation disrupts axon growth and synaptic stability and impairs spatial learning and memory [47]. In addition, ANGPTL8 treatment induced an increase in the activity of cofilin, reflected by its lower phosphorylation status. As a downstream effector of ROCK, high cofilin activity can inhibit the extension of neurites [17, 47]. Moreover, ANGPTL8-induced destruction of neuronal network structure and damage to axons and synapses were eliminated by blocking PirB or inhibiting its downstream signals. These findings are consistent with previous studies indicating that blocking PirB reverses the inhibition of neurite outgrowth [54] and that PirB may be involved in the modulation of synaptic plasticity through ROCK2/cofilin signaling [17, 26, 63, 64].

Similarly, to elucidate the underlying mechanisms of ANGPTL8-induced neuroinflammation, we detected inflammatory signals and found that the NF-κB, AKT, ERK1/2, and P38 signaling pathways in microglia strongly responded to ANGPTL8 stimulation. Moreover, ANGPTL8-induced inflammation was abrogated by PirB blockade with neutralizing antibodies and inhibitors of P38 and P65, further indicating that ANGPTL8-associated signals are downstream of PirB. These results are consistent with previous studies showing that PirB regulates the phosphorylation of AKT, ERK1/2, P38, and P65 [56].

Furthermore, *PirB*$^{-/-}$ mice were used to further confirm the role of PirB in vivo in this study. The results showed that knockout of *PirB* reduced neuroinflammation, alleviated neuronal damage, and improved cognitive dysfunction induced by ANGPTL8. These findings shed mechanistic light on previous studies suggesting that PirB participates in a key pathological process of the nervous system, specifically axonal regeneration inhibition in mediating cognitive decline [16, 17]. This suggests that targeting ANGPTL8-PirB axis signaling may provide a therapeutic strategy for diabetes-associated cognitive dysfunction.

Nevertheless, there are several limitations to consider in this study. First, the molecular mechanism by which the expression of ANGPTL8 in neurons is increased should be identified. Second, we did not perform studies in female mice. Moreover, our study focused on the plasticity of the neural structure, but whether such neuromorphological alterations are accompanied by functional changes remains to be identified in our next work.

Collectively, ANGPTL8-PirB is an important signaling axis for the pathogenesis of diabetes-associated cognitive dysfunction via crosstalk between neurons and microglia. It is possible that increased ANGPTL8 levels in the diabetic hippocampus result in the exacerbation of neuronal damage, the induction of microglial polarization, and the enhancement of neuroinflammation. Thus, blocking the binding of ANGPTL8 to PirB may be a promising strategy for the management of diabetes-associated cognitive dysfunction that reduces inflammation and preserves neuronal function. In conclusion, this study reveals a previously unrecognized role of ANGPTL8 in the pathogenesis of diabetes-associated cognitive dysfunction and identifies the ANGPTL8-PirB signaling pathway as a potential target for the management of diabetes-associated cognitive dysfunction in the future.

Abbreviations

T2D	Type 2 diabetes mellitus
ANGPTL8	Angiopoietin-like protein 8
PirB	Paired immunoglobulin-like receptor B
RIFL	Refeeding induced in fat and liver
LILRB	Leukocyte immunoglobulin-like receptor B
CNS	Central nervous system
MMSE	Mini-Mental State Examination
MoCA	Montreal cognitive assessment
MCI	Mild cognitive impairment
CSF	Cerebrospinal fluid
WT	Wild-type
Angptl8^{Nestin} *CKO*	CNS-specific *Angptl8*-depletion
cKO	Conditional knockout
gRNA	Guide RNA
PirB$^{-/-}$	PirB knockout
HFD	High-fat diet
ND	Normal diet
rA8	Recombinant ANGPTL8 protein
min	Minute
GTT	Glucose tolerance test
ITT	Insulin tolerance test
LPS	Lipopolysaccharide
rA8-flag	Flag-targeted recombinant ANGPTL8 protein
i.p.	Intraperitoneally
qPCR	Quantitative polymerase chain reaction
ELISA	Enzyme-linked immunosorbent assay
TG	Triglyceride
pAbs	Primary antibodies
mAb	Monoclonal antibody
PBS	Phosphate-buffered saline
DAPI	4′,6-Diamidino-2-phenylindole
PFA	Paraformaldehyde
PLL	Poly-L-lysine
DMEM/F12	Dulbecco's modified Eagle's medium/nutrient mixture F-12
FBS	Fetal bovine serum
FC	Fold change

BSA	Bovine serum albumin
RT–qPCR	Real-time quantitative PCR
PVDF	Polyvinylidene fluoride
TBST	Tris-buffered saline containing Tween-20
BMI	Body mass index
Gap-43	Growth-associated protein-43
Snap-25	Synaptosomal-associated protein 25
Nfl	Neurofilament light chain
Syp	Synaptophysin
LTP	Long-term potentiation
HbA1c	Glycated hemoglobin

Supplementary Information

The online version contains supplementary material available at https://doi.org/10.1186/s12974-024-03183-8.

Supplementary Material 1.

Supplementary Material 2.

Supplementary Material 3.

Acknowledgements
We would like to thank all the participants in the study.

Author contributions
X.M., D.L., Y.Y. and X.Y. participated in the research design. X.M., D.L., and R.K. conducted the experiments. Y.X., L.P., Y.G., P.Y., P.L., H.Z., L.H., Y.Z., B.M., Y.H., L.X., J.X., X.L., W.L., Y.C., S.Z. contributed to data analysis and interpretation. X.M. and D.L. drafted the paper. X.Y. and Y.Y. supervised the study and revised the paper. All authors contributed to the paper and approved the final manuscript.

Funding
This work was supported by Grants from the National Natural Science Foundation of China (82270880, 81974109 and 81570740).

Availability of data and materials
All data needed to evaluate the conclusions in the manuscript are present in the manuscript and the supplementary Materials. All methods and protocols used are included in the main manuscript or supplementary files. All reagents, antibodies, and resources are listed in the main manuscript. The data sets used and/or analyzed during the current study are available from the corresponding authors on reasonable request.

Declarations

Ethics approval and consent to participate
The study protocols of participants (approval number: TJ-IRB20230452) were approved by the Committee on Human Research at Tongji Hospital, Tongji Medical College, Huazhong University of Science and Technology. All animal protocols were approved by the Institutional Animal Care and Use Committee of the Institute of Model Animals of Tongji Hospital, Huazhong University of Science and Technology. The animals received humane care according to the criteria outlined in the Guide for the Care and Use of Laboratory Animals prepared by the National Academy of Sciences and published by the National Institutes of Health.

Consent for publication
Not applicable.

Competing interests
The authors declare no competing interests.

Author details
[1]Division of Endocrinology, Department of Internal Medicine, Tongji Hospital, Tongji Medical College, Huazhong University of Science and Technology, Wuhan 430030, China. [2]Branch of National Clinical Research Center for Metabolic Diseases, Wuhan, Hubei, China. [3]Department of Neurology, Tongji Hospital, Tongji Medical College, Huazhong University of Science and Technology, Wuhan, China. [4]Computer Center, Tongji Hospital, Tongji Medical College, Huazhong University of Science and Technology, Wuhan, China.

Received: 22 January 2024 Accepted: 22 July 2024
Published online: 02 August 2024

References

1. Zhang J, et al. An updated meta-analysis of cohort studies: diabetes and risk of Alzheimer's disease. Diabetes Res Clin Pract. 2017;124:41–7. https://doi.org/10.1016/j.diabres.2016.10.024.
2. Moheet A, Mangia S, Seaquist ER. Impact of diabetes on cognitive function and brain structure. Ann N Y Acad Sci. 2015;1353:60–71. https://doi.org/10.1111/nyas.12807.
3. Biessels GJ, et al. Cerebral function in diabetes mellitus. Diabetologia. 1994;37:643–50. https://doi.org/10.1007/BF00417687.
4. Magarinos AM, McEwen BS. Experimental diabetes in rats causes hippocampal dendritic and synaptic reorganization and increased glucocorticoid reactivity to stress. Proc Natl Acad Sci USA. 2000;97:11056–61. https://doi.org/10.1073/pnas.97.20.11056.
5. Kamal A, Biessels GJ, Urban IJ, Gispen WH. Hippocampal synaptic plasticity in streptozotocin-diabetic rats: impairment of long-term potentiation and facilitation of long-term depression. Neuroscience. 1999;90:737–45. https://doi.org/10.1016/s0306-4522(98)00485-0.
6. Li ZG, Zhang W, Grunberger G, Sima AA. Hippocampal neuronal apoptosis in type 1 diabetes. Brain Res. 2002;946:221–31. https://doi.org/10.1016/s0006-8993(02)02887-1.
7. Zilliox LA, Chadrasekaran K, Kwan JY, Russell JW. Diabetes and cognitive impairment. Curr DiabRep. 2016;16:87. https://doi.org/10.1007/s11892-016-0775-x.
8. Sheppard O, Coleman MP, Durrant CS. Lipopolysaccharide-induced neuroinflammation induces presynaptic disruption through a direct action on brain tissue involving microglia-derived interleukin 1 beta. J Neuroinflamm. 2019;16:106. https://doi.org/10.1186/s12974-019-1490-8.
9. Navaeian M, Asadian S, Ahmadpour Yazdi H, Gheibi N. ANGPTL8 roles in proliferation, metabolic diseases, hypothyroidism, polycystic ovary syndrome, and signaling pathways. Mol Biol Rep. 2021;48:3719–31. https://doi.org/10.1007/s11033-021-06270-8.
10. Abu-Farha M, et al. The multi-faces of Angptl8 in health and disease: novel functions beyond lipoprotein lipase modulation. Prog Lipid Res. 2020;80:101067. https://doi.org/10.1016/j.plipres.2020.101067.
11. Chen X, et al. Circulating betatrophin levels are increased in patients with type 2 diabetes and associated with insulin resistance. J Clin Endocrinol Metab. 2015;100:E96-100. https://doi.org/10.1210/jc.2014-2300.
12. Xu J, et al. The correlation between circulating betatrophin and insulin resistance in general population: a meta-analysis. Horm Metabol Res. 2017;49:760–71. https://doi.org/10.1055/s-0043-108911.
13. Wang R, et al. Neuropeptide Y-positive neurons in the dorsomedial hypothalamus are involved in the anorexic effect of Angptl8. Front Mol Neurosci. 2018;11:451. https://doi.org/10.3389/fnmol.2018.00451.
14. Quagliarini F, et al. Atypical angiopoietin-like protein that regulates ANGPTL3. Proc Natl Acad Sci USA. 2012;109:19751–6. https://doi.org/10.1073/pnas.1217552109.
15. Li DP, et al. LILRB2/PirB mediates macrophage recruitment in fibrogenesis of nonalcoholic steatohepatitis. Nat Commun. 2023;14:4436. https://doi.org/10.1038/s41467-023-40183-3.
16. Liu J, Wang Y, Fu W. Axon regeneration impediment: the role of paired immunoglobulin-like receptor B. Neural Regen Res. 2015;10:1338–42. https://doi.org/10.4103/1673-5374.162771.
17. Kim T, et al. Human LilrB2 is a beta-amyloid receptor and its murine homolog PirB regulates synaptic plasticity in an Alzheimer's model. Science. 2013;341:1399–404. https://doi.org/10.1126/science.1242077.
18. Starkey HDV, et al. Neuroglial expression of the MHCI pathway and PirB receptor is upregulated in the hippocampus with advanced aging. J Mol Neurosci. 2012;48:111–26. https://doi.org/10.1007/s12031-012-9783-8.
19. Folstein MF, Folstein SE, McHugh PR. "Mini-mental state": a practical method for grading the cognitive state of patients for the clinician. J

Psychiatr Res. 1975;12:189–98. https://doi.org/10.1016/0022-3956(75)90026-6.
20. Nasreddine ZS, et al. The montreal cognitive assessment, MoCA: a brief screening tool for mild cognitive impairment. J Am Geriatr Soc. 2005;53:695–9. https://doi.org/10.1111/j.1532-5415.2005.53221.x.
21. Moyer VA, US Preventive Services Task Force. Screening for cognitive impairment in older adults: U.S. preventive services task force recommendation statement. Ann Intern Med. 2014;160:791–7. https://doi.org/10.7326/M14-0496.
22. Tsoi KK, et al. Cognitive tests to detect dementia: a systematic review and meta-analysis. JAMA Intern Med. 2015;175:1450–8. https://doi.org/10.1001/jamainternmed.2015.2152.
23. Guide for the care and use of laboratory animals. 1996.
24. Guillemot-Legris O, et al. High-fat diet feeding differentially affects the development of inflammation in the central nervous system. J Neuroinflammation. 2016;13:206. https://doi.org/10.1186/s12974-016-0666-8.
25. Petrov D, et al. High-fat diet-induced deregulation of hippocampal insulin signaling and mitochondrial homeostasis deficiences contribute to Alzheimer disease pathology in rodents. Biochim Biophys Acta. 2015;1852:1687–99. https://doi.org/10.1016/j.bbadis.2015.05.004.
26. Pu K, et al. Involvement of paired immunoglobulin-like receptor B in diabetes-associated cognitive dysfunction through modulation of axon outgrowth and dendritic remodeling. Mol Neurobiol. 2022;59:2563–79. https://doi.org/10.1007/s12035-021-02679-1.
27. Huang J, et al. Disruption of circadian clocks promotes progression of Alzheimer's disease in diabetic mice. Mol Neurobiol. 2021;58:4404–12. https://doi.org/10.1007/s12035-021-02425-7.
28. Peng X, et al. Time-restricted feeding rescues circadian disruption-aggravated progression of Alzheimer's disease in diabetic mice. J Nutr Biochem. 2022;110: 109128. https://doi.org/10.1016/j.jnutbio.2022.109128.
29. Yang Y, et al. Exendin-4 reduces food intake via the PI3K/AKT signaling pathway in the hypothalamus. Sci Rep. 2017;7:6936. https://doi.org/10.1038/s41598-017-06951-0.
30. Barbash S, Hanin G, Soreq H. Stereotactic injection of microRNA-expressing lentiviruses to the mouse hippocampus ca1 region and assessment of the behavioral outcome. J Vis Exp. 2013. https://doi.org/10.3791/50170.
31. Jeong EA, et al. Tonicity-responsive enhancer-binding protein promotes diabetic neuroinflammation and cognitive impairment via upregulation of lipocalin-2. J Neuroinflammation. 2021;18:278. https://doi.org/10.1186/s12974-021-02331-8.
32. Volmar CH, et al. M344 promotes nonamyloidogenic amyloid precursor protein processing while normalizing Alzheimer's disease genes and improving memory. Proc Natl Acad Sci USA. 2017;114:E9135–44. https://doi.org/10.1073/pnas.1707544114.
33. Fruhauf PK, et al. Spermine reverses lipopolysaccharide-induced memory deficit in mice. J Neuroinflammation. 2015;12:3. https://doi.org/10.1186/s12974-014-0220-5.
34. Sasaki F, et al. A high-affinity monoclonal antibody against the FLAG tag useful for G-protein-coupled receptor study. Anal Biochem. 2012;425:157–65. https://doi.org/10.1016/j.ab.2012.03.014.
35. Liu H, et al. SARM1 promotes neuroinflammation and inhibits neural regeneration after spinal cord injury through NF-kappaB signaling. Theranostics. 2021;11:4187–206. https://doi.org/10.7150/thno.49054.
36. Osen-Sand A, et al. Inhibition of axonal growth by SNAP-25 antisense oligonucleotides in vitro and in vivo. Nature. 1993;364:445–8. https://doi.org/10.1038/364445a0.
37. Hou Q, et al. SNAP-25 in hippocampal CA1 region is involved in memory consolidation. Eur J Neurosci. 2004;20:1593–603. https://doi.org/10.1111/j.1460-9568.2004.03600.x.
38. Luo R, et al. Activation of PPARA-mediated autophagy reduces Alzheimer disease-like pathology and cognitive decline in a murine model. Autophagy. 2020;16:52–69. https://doi.org/10.1080/15548627.2019.1596488.
39. Benowitz LI, Routtenberg A. GAP-43: an intrinsic determinant of neuronal development and plasticity. Trends Neurosci. 1997;20:84–91. https://doi.org/10.1016/s0166-2236(96)10072-2.
40. Sandelius A, et al. Elevated CSF GAP-43 is Alzheimer's disease specific and associated with tau and amyloid pathology. Alzheimer's Dement. 2019;15:55–64. https://doi.org/10.1016/j.jalz.2018.08.006.
41. Zhang Y, et al. Growth-associated protein GAP-43 and L1 act synergistically to promote regenerative growth of Purkinje cell axons in vivo. Proc Natl Acad Sci USA. 2005;102:14883–8. https://doi.org/10.1073/pnas.0505164102.
42. Svenningsson AL, et al. Axonal degeneration and amyloid pathology predict cognitive decline beyond cortical atrophy. Alzheimer's Res Ther. 2022;14:144. https://doi.org/10.1186/s13195-022-01081-w.
43. Mattsson N, et al. Association between longitudinal plasma neurofilament light and neurodegeneration in patients with Alzheimer disease. JAMA Neurol. 2019;76:791–9. https://doi.org/10.1001/jamaneurol.2019.0765.
44. Pereira JB, et al. Untangling the association of amyloid-beta and tau with synaptic and axonal loss in Alzheimer's disease. Brain. 2021;144:310–24. https://doi.org/10.1093/brain/awaa395.
45. McLeod VM, et al. Exploring germline recombination in Nestin-Cre transgenic mice using floxed androgen receptor. Genesis. 2020;58: e23390. https://doi.org/10.1002/dvg.23390.
46. Takai T. Paired immunoglobulin-like receptors and their MHC class I recognition. Immunology. 2005;115:433–40. https://doi.org/10.1111/j.1365-2567.2005.02177.x.
47. Lu W, Wen J, Chen Z. Distinct roles of ROCK1 and ROCK2 on the cerebral ischemia injury and subsequently neurodegenerative changes. Pharmacology. 2020;105:3–8. https://doi.org/10.1159/000502914.
48. Wang J, et al. Extracellular vesicles mediate the communication of adipose tissue with brain and promote cognitive impairment associated with insulin resistance. Cell Metab. 2022;34:1264-1279e1268. https://doi.org/10.1016/j.cmet.2022.08.004.
49. Yamada H, et al. Circulating betatrophin is elevated in patients with type 1 and type 2 diabetes. Endocr J. 2015;62:417–21. https://doi.org/10.1507/endocrj.EJ14-0525.
50. Ehtewish H, Arredouani A, El-Agnaf O. Diagnostic, prognostic, and mechanistic biomarkers of diabetes mellitus-associated cognitive decline. Int J Mol Sci. 2022. https://doi.org/10.3390/ijms23116144.
51. Liao Z, et al. Angiopoietin-like protein 8 expression and association with extracellular matrix metabolism and inflammation during intervertebral disc degeneration. J Cell Mol Med. 2019;23:5737–50. https://doi.org/10.1111/jcmm.14488.
52. McCrimmon RJ, Ryan CM, Frier BM. Diabetes and cognitive dysfunction. Lancet. 2012;379:2291–9. https://doi.org/10.1016/S0140-6736(12)60360-2.
53. Lu P, et al. Insulin upregulates betatrophin expression via PI3K/Akt pathway. Sci Rep. 2017;7:5594. https://doi.org/10.1038/s41598-017-06052-y.
54. Atwal JK, et al. PirB is a functional receptor for myelin inhibitors of axonal regeneration. Science. 2008;322:967–70. https://doi.org/10.1126/science.1161151.
55. Filbin MT. PirB, a second receptor for the myelin inhibitors of axonal regeneration Nogo66, MAG, and OMgp: implications for regeneration in vivo. Neuron. 2008;60:740–2. https://doi.org/10.1016/j.neuron.2008.12.001.
56. Chen S, et al. Angptl8 mediates food-driven resetting of hepatic circadian clock in mice. Nat Commun. 2019. https://doi.org/10.1038/s41467-019-11513-1.
57. Hu L, et al. ANGPTL8 is a negative regulator in pathological cardiac hypertrophy. Cell Death Dis. 2022;13:621. https://doi.org/10.1038/s41419-022-05029-8.
58. Houchin-Ray T, Zelivyanskaya M, Huang A, Shea LD. Non-viral gene delivery transfection profiles influence neuronal architecture in an in vitro co-culture model. Biotechnol Bioeng. 2009;103:1023–33. https://doi.org/10.1002/bit.22311.
59. Mittenbühler MJ, et al. Isolation of extracellular fluids reveals novel secreted bioactive proteins from muscle and fat tissues. Cell Metab. 2023;35:535-549.e537. https://doi.org/10.1016/j.cmet.2022.12.014.
60. Dove A, et al. The impact of diabetes on cognitive impairment and its progression to dementia. Alzheimer's Dement. 2021;17:1769–78. https://doi.org/10.1002/alz.12482.
61. Zhang Y, et al. ANGPTL8 negatively regulates NF-kappaB activation by facilitating selective autophagic degradation of IKKgamma. Nat Commun. 2017;8:2164. https://doi.org/10.1038/s41467-017-02355-w.
62. Yang Y, et al. Increased circulating angiopoietin-like protein 8 levels are associated with thoracic aortic dissection and higher inflammatory

conditions. Cardiovasc Drugs Ther. 2020;34:65–77. https://doi.org/10.1007/s10557-019-06924-7.
63. Zhang Z, et al. A screened PirB antagonist peptide antagonizes Abeta(42)-mediated inhibition of neurite outgrowth in vitro. Appl Microbiol Biotechnol. 2021;105:4649–62. https://doi.org/10.1007/s00253-021-11363-2.
64. Gou Z, et al. PirB is a novel potential therapeutic target for enhancing axonal regeneration and synaptic plasticity following CNS injury in mammals. J Drug Target. 2014;22:365–71. https://doi.org/10.3109/1061186X.2013.878939.

Publisher's Note